Title: Calibration Requirements	**Owner:** C. Hales	**Date:** 2020-11-30
NRAO Doc. #: 020.22.00.00.00-0001-REQ-C-ARRAY_CALIBRATION_REQS		**Version:** C

Calibration Requirements

020.22.00.00.00-0001-REQ-C-ARRAY_CALIBRATION_REQS

Status: **RELEASED**

PREPARED BY	ORGANIZATION	DATE
C. Hales	Electronics Div., NRAO	2020-11-30

APPROVALS	ORGANIZATION	SIGNATURES
R. Selina, Project Engineer	Electronics Div., NRAO	Digitally signed by Robert Selina Date: 2020.11.30 15:10:01 -07'00'
E. Murphy, Project Scientist	NM-Operations, NRAO	Digitally signed by Eric J. Murphy Date: 2020.12.05 13:44:12 -05'00'
T. Kusel, System Engineer	PMD, NRAO	Thomas Kusel Digitally signed by Thomas Kusel Date: 2020.12.08 15:41:46 +02'00'
R. Farnsworth, Project Manager	PMD, NRAO	Richard L Farnsworth Digitally signed by Richard L Farnsworth Date: 2020.12.14 17:02:13 -05'00'

RELEASED BY	ORGANIZATION	SIGNATURE
R. Farnsworth, Project Manager	PMD, NRAO	Richard L Farnsworth Digitally signed by Richard L Farnsworth Date: 2020.12.14 17:02:32 -05'00'

Change Record

Version	Date	Author	Affected Sections	Reason
01	2018-11-01	Hales	All	Initial framework based on ALMA Calibration Specifications and Requirements [RD01].
02	2019-05-28	Hales	All	First complete draft.
03	2019-07-12	Hales	1,6	Minor clarifications and corrections following review by the Calibration Working Group. Revised pointing requirements.
A	2019-08-02	Hales, Lear	All	Updated cover page and headers in preparation for approvals and release.
A.01	2019-08-09	Hales	5	Updated traceability column.
A.02	2019-12-20	Hales	All	Updated all calculations and requirements to satisfy new dynamic range limits in Version B of the Science Requirements.
A.03	2020-05-07	Hales	All	Updated dynamic range calculations and all derived quantities. Added requirements for the Short Baseline Array.
A.04	2020-05-27	Hales	All	Minor updates following review by TAC, R. Selina, E. Murphy, and B. Butler. Removed L1 requirements, revised traceability. Clarified introductory material. Expanded summary.
B	2020-06-22	Hales, Lear	All	Minor updates. Prepared document for approvals and release.
C	2020-11-30	Hales, Lear	5.3, 5.4.2, 5.8, 6	Revised delay noise requirements. Added verification section. Prepared document for approvals and release.

Table of Contents

1 INTRODUCTION

1.1 Purpose

This document presents requirements for calibration capabilities of the ngVLA.

This document does *not* present calibration strategies for specific observing modes nor requirements for implementing these strategies (as may be anticipated by a scientist). Instead, this document focuses on requirements that are necessary to appropriately design the instrument so as to support the multitude of calibration strategies that will be performed to deliver scientifically useful data across a variety of observing modes. The key aim of this document is to ensure that whatever calibration strategies are needed to deliver specific observing modes, a sufficiently capable ngVLA system will exist to support implementation of these strategies to within acceptable levels of performance. There is a future need to define calibration strategies and their implementation requirements (pipeline calibration requirements) for science observing modes, but this is beyond the scope of this document.

The calibration requirements presented in this document flow-down without exception from the ngVLA System Requirements [AD03]. The System Requirements are in turn derived from the ngVLA Science Requirements [AD01] and ngVLA Stakeholder Requirements [AD02].

The requirements presented in this document will guide aspects of the facility design including hardware, software, and operational elements.

Some revisions to the System Requirements are anticipated as the facility concept matures. Similarly, the Science and Stakeholder Requirements may change depending on the degree of alignment with the National Academy of Sciences Astro 2020 Decadal Survey goals. As these changes occur, updates will be made to this document.

1.2 Scope

The scope of this document is the set of key quantities that will need to be measured or taken into account in order to collect and calibrate ngVLA data.

This document does *not* explicitly address all calibration parameter space. Instead, it focuses on key aspects of calibration that drive design and are necessary to support the higher-level science, stakeholder, and system requirements. These in turn yield implicit constraints on performance throughout the remaining parameter space.

This document does *not* explicitly define observing modes, nor calibration strategies for particular observing modes, nor does it lay out work for commissioning, operating, or maintaining the telescope. This document does, however, provide foundations for addressing/constraining each of these aspects.

For context, the suite of standard ngVLA observing modes is currently under development [AD11]. These are defined as the subset of all possible observing modes for which end-to-end functionality from PI proposal submission to output Science Ready Data Products will be a construction project deliverable, and for which the calibration and data processing will be undertaken through a fully automated pipeline developed and run by the Observatory. Each standard observing mode will effectively identify a list of rules that every subsystem must follow in order for the requested data product to be successful, including calibration strategies which have yet to be formally developed. Observing modes for the ngVLA will employ various configurations of the 9 functional operating modes defined in the System Requirements [AD03]. These are: Interferometric, Phased Array, Pulsar Timing, Pulsar and Transient Search, VLBI, Total Power, On-The-Fly Mapping, Solar, and Concurrent Interferometric and Phased Array. The commensality matrix for these operating modes is presented in AD03.

This document represents a snaphot in time in the design evolution of the ngVLA. Any differences or inconsistencies between the requirements derived in this document and capabilities presented elsewhere in the ngVLA documentation suite will form the basis for future decisions as the facility concept matures.

This document currently focuses primarily on Interferometric requirements for ngVLA. Future updates to this document are anticipated in which each of the functional operating modes above, some of which have been implicitly considered when developing requirements in this version, will be explicitly addressed.

2 RELATED DOCUMENTS

2.1 Applicable Documents

The following documents apply to this Requirements Specification to the extent specified. In the event of a conflict between the documents referenced herein and the content of this Requirements Specification, the content of the highest level specification (in the requirements flow-down) shall be considered the superseding requirement for design elaboration and verification.

Reference No.	Document Title	Rev. / Doc. No.
AD01	ngVLA Science Requirements	020.10.15.05.00-0001-REQ
AD02	ngVLA Stakeholder Requirements	020.10.15.01.00-0001-REQ
AD03	ngVLA System Requirements	020.10.15.10.00-0003-REQ
AD04	ngVLA System Reference Design	020.10.20.00.00-001-REP
AD05	ngVLA Operations Concept	020.10.05.00.00-0002-PLA

Reference No.	Document Title	Rev. / Doc. No.
AD06	ngVLA Environmental Specifications	020.10.15.10.00-0001-SPE
AD07	ngVLA Reference Observing Program	020.10.15.05.10-0001-SPE
AD08	ngVLA EMC Compatibility and RFI Mitigation Requirements	020.10.15.10.00-0002-REQ
AD09	ngVLA Requirements Management Plan	020.10.15.00.00-0001-PLA
AD10	ngVLA Front End Reference Design Description	020.30.03.00.00-0002-DSN
AD11	ngVLA Observing Modes Concept	020.10.05.05.00-0005-PLA
AD12	ngvla Front End Technical Requirements	020.30.03.01.00-0001-REQ
AD13	ngVLA Integrated Receivers and Downconverters: Technical Requirements	020.30.15.00.00-0001-REQ

2.2 Reference Documents

The following references provide supporting context.

Reference No.	Document Title	Rev. / Doc. No.
RD01	ALMA Calibration Specifications and Requirements (Version D, 5/18/2006)	ALMA-90.03.00.00-001-A-SPE
RD02	Taperability Study for the ngVLA and Performance Estimates	Rosero, 2019, ngVLA Memo 55
RD03	Image Dynamic Range Limits Arising From Visibility Errors	Hales, 2019, ngVLA Memo 60
RD04	Antenna Tolerance Theory – A Review	Ruze, 1966, Proc. IEEE, 54, 633
RD05	The Primary Antenna Elements	Napier, 1999, Synthesis Imaging in Radio Astronomy II, 180, 37
RD06	Fast Switching Phase Calibration at 3mm at the VLA Site	Carilli, 2015, ngVLA Memo 1
RD07	Interferometry and Synthesis in Radio Astronomy	Thompson, Moran & Swenson, 2017, Springer, 3rd Ed.
RD08	Microarcsecond Radio Astronomy	Reid & Honma, 2014, ARAA, 52, 339
RD09	Astrometric Effects of Secular Aberration	Kopeikin & Makarov, 2006, AJ, 131, 1471
RD10	A new concept of the International Celestial Reference Frame: the epoch ICRF	Xu et al., 2013, MNRAS, 430, 2633

Reference No.	Document Title	Rev. / Doc. No.
RD11	The pointing self calibration algorithm for aperture synthesis radio telescopes	Bhatnagar & Cornwell, 2017, AJ, 154, 197B
RD12	Wide-field wide-band Interferometric Imaging: The WB A-Projection and Hybrid Algorithms	Bhatnagar et al., 2013, ApJ, 770, 91
RD13	Requirements for Subreflector and Feed Positioning for ALMA Antennas	Butler, 2003, ALMA Memo 479
RD14	Temporal and Spatial Tropospheric Phase Fluctuations at the VLA (and Beyond) and Implications for Phase Calibration	Hales, 2019, ngVLA Memo 61
RD15	Calibration Errors in Interferometric Radio Polarimetry	Hales, 2017, AJ, 154, 54
RD16	Phase calibration and water vapor radiometry for millimeter-wave arrays	Lay, 1997, A&AS, 122, 547
RD17	Astrometry and Geodesy with Radio Interferometry: Experiments, Models, Results	Sovers et al., 1998, Rev. Mod. Phys., 70, 1393
RD18	Temporal and Spatial Ionospheric Phase Fluctuations at the VLA (and Beyond) and Implications for Phase Calibration	Hales, 2020, ngVLA Memo 62 (in prep.)
RD19	Spectra of L-band ionospheric scintillation over Nanjing	Fang et al., 2012, Chin. Sci. Bull., 57, 3375
RD20	A Search For Sub-Second Radio Variability Predicted To Arise Toward 3C84 From Intergalactic Dispersion	Hales et al., 2016, ApJ, 823, 93
RD21	Measurement of the Parallax of PSR B0950+08 Using the VLBA	Brisken et al., 2000, ApJ, 541, 959
RD22	An ionospheric index suitable for estimating the degree of ionospheric perturbations	Wilken et al., 2018, J. Space Weather Space Clim., 8, A19
RD23	How Close to the Sun Should We Observe With the VLA?	Butler, 2005, VLA Test Memo 236
RD24	An Accurate Flux Density Scale from 1 to 50 GHz	Perley & Butler, 2013, ApJS, 204, 19
RD25	Flux Density Models for Solar System Bodies In CASA	Butler, 2012, ALMA Memo 594
RD26	Atmospheric Opacity at the VLA	Uson, 1986, VLA Sci. Memo 157
RD27	Temporal and Spatial Tropospheric Opacity Fluctuations at the VLA (and Beyond) and Implications for Amplitude Calibration	Hales, 2020, ngVLA Memo 63 (in prep.)

Reference No.	Document Title	Rev. / Doc. No.
RD28	On Determining Visibilities from Correlation Products	Perley, 2010, EVLA Memo 145
RD29	The ALMA Calibrator Database I: Measurements Taken During the Commissioning Phase of ALMA	van Kempen et al., 2014, ALMA Memo 599
RD30	Understanding radio polarimetry. II. Instrumental calibration of an interferometer array	Sault et al., 1996, A&AS, 117, 149
RD31	CASA Interferometric Pipeline Polarization Calibration & Imaging Requirement & Design Specifications	Hales, 2017, ALMA Memo 603
RD32	Radio circular polarization of active galaxies	Rayner et al., 2000, MNRAS, 319, 484
RD33	The Synthesis Radio Telescope at Westerbork. Methods of Polarization Measurement	Weiler, 1973, A&A, 26, 403
RD34	Determining full EVLA polarization leakage terms at C and X bands	Sault & Perley, 2013, EVLA Memo 170
RD35	Integrated Polarization Properties of 3C48, 3C138, 3C147, and 3C286	Perley & Butler, 2013, ApJS, 206, 16
RD36	Polarimetric calibration and dynamic range issues	Sault & Perley, 2014, EVLA Memo 177
RD37	Dipole Alignment Tolerance for the JVLA's Low-Band System	Perley, 2016, EVLA Memo 200
RD38	ALMA EOC Polarization Commissioning Report	Cortes et al., 2015, ALMA Tech. Note (draft version Nov 23)
RD39	Polarization Calibration of the VLBA Using the D-terms	Gomez et al., 2002, VLBA Sci. Memo 30
RD40	JVLA calibration stability at L-band over 5.5 years	Hales & Stephenson, 2019, EVLA Memo 208
RD41	Dual differential polarimetry. A technique to recover polarimetric information from dual-polarization observations	Marti-Vidal et al., 2016, A&A, 593, A61
RD42	Direction-dependent Corrections in Polarimetric Radio Imaging. I. Characterizing the Effects of the Primary Beam on Full-Stokes Imaging	Jagannathan et al., 2017, AJ, 154, 56

Reference No.	Document Title	Rev. / Doc. No.
RD43	Dynamic range loss due to the retarded baseline effect	Voronkov & Wieringa, 2005, SKA Memo 68
RD44	Demonstration & Analysis of ngVLA core + Short Baseline Array Extended Structure Imaging	Mason, 2019, ngVLA Memo 67
RD45	The ngVLA Short Baseline Array	Mason et al., 2018, ngVLA Memo 43
RD46	Image Corruption from Antenna Pointing Errors: Simulation Results (and Useful Teaching Tool)	Hales, 2020, ngVLA Memo 75

3 REQUIREMENTS MANAGEMENT

3.1 Requirements Definitions

Requirement Level	Definition
L0	User requirements expressed in terms applicable to their needs or use cases ("Science Requirements" or "Stakeholder Requirements")
L1	Requirements expressed in technical functional or performance terms, but still implementation agnostic ("System Level Requirements")
L1.1	Same as L1, but with a presumed achitecture ("System Level Requirements")
L2	Requirements that define a specification for an element of the system, presuming an architecture ("Sub System Requirements")

3.2 Requirements Flow-Down

The requirements flow-down to this document is displayed in Figure 1.

The Science Requirements [AD01] and Stakeholder Requirements [AD02], including their subsidiaries, fully encapsulate all known L0 requirements for the facility. The L1 System Requirements [AD03] flow from the L0 Science Requirements and L0 Stakeholder Requirements. The System Requirements and subsidiaries [e.g. AD06, AD08] fully encapsulates all known L1 requirements.

This document presents Level 1.1 requirements. These are system level requirements that provide

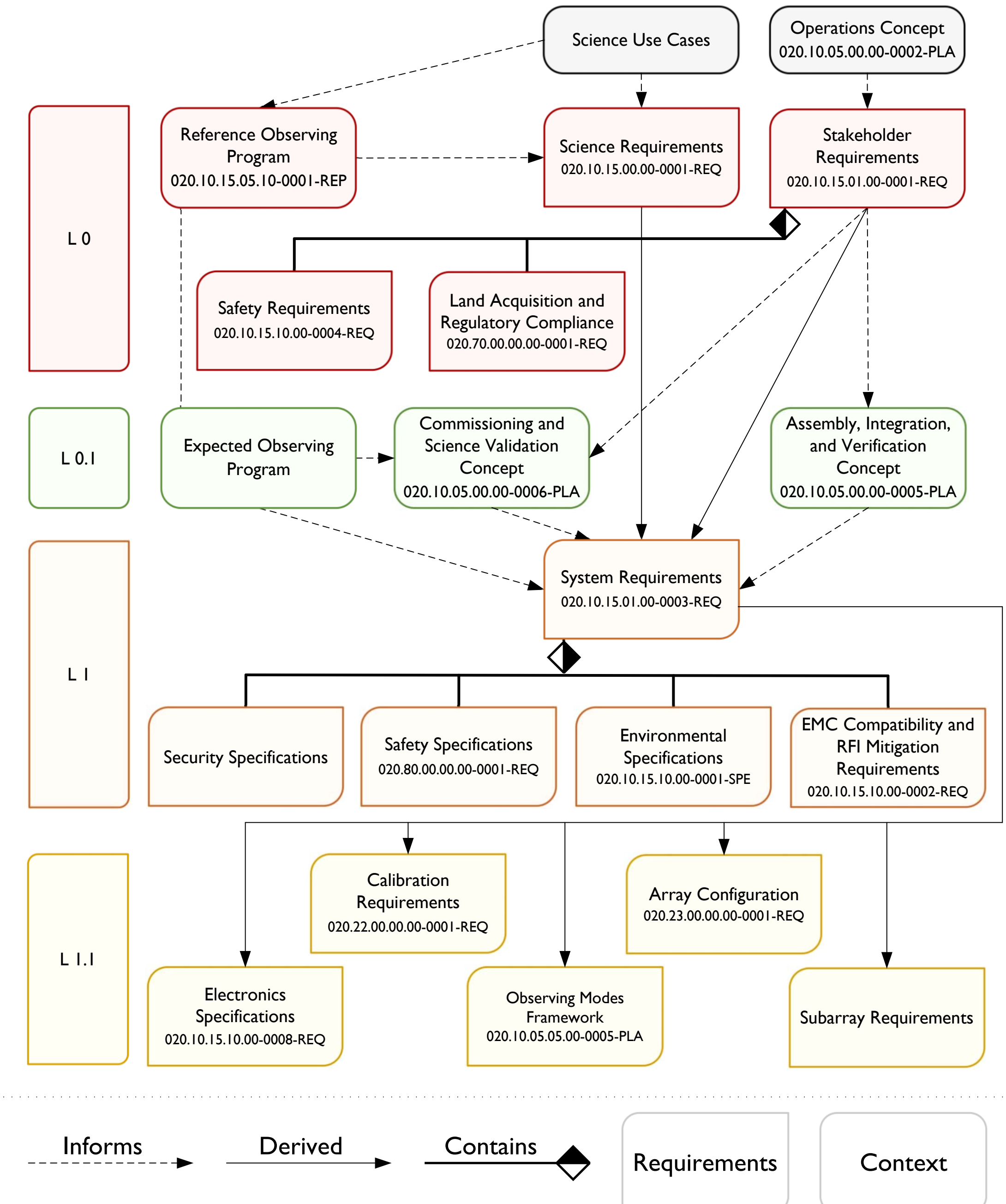

Figure 1 Requirements flow-down. This document presents a subset of Level 1.1 requirements.

derivations for L2 sub-systems, but with the important distinction that they presume an architecture. L1.1 requirements are subordinate to formal L1 system requirements.

Individual sub-system requirements (L2) flow from the L1 and L1.1 system-level requirements, and may not always be directly attributable to a single system-level requirement. For example, phase drift specifications at the system level may be apportioned to multiple sub-systems, or a sub-system specification may be in support of multiple higher-level requirements. Completeness of the L2 requirements is assessed at the requirements review of each sub-system.

While this is a top-down design process, the process is still iterative rather than a 'waterfall' or linear process. The feasibility and cost of implementation of requirements and specifications lead to trade-offs that feed back to higher-level requirements. The end goal is to build the most generally capable system within the programmatic constraints of cost and schedule.

Maintaining enumerated and traceable science requirements, system requirements, and sub-system specifications ensures this trade-off process is complete and well understood by the project team. The effect of a change in a sub-system specification can be analyzed at the system level, and thereafter the impact on a specific scientific program can be ascertained.

Details of the requirements management strategy can be found in AD09.

3.3 Verb Convention

This document uses 'shall' to denote a requirement and 'goal' to denote a feature that is desired but not required. Where 'goal' is not explicitly included in the definition, its usage will be implied by 'desired'.

4 OVERVIEW OF CALIBRATION REQUIREMENTS

Calibration is the process of removing corrupting effects from measured data, with the aim to produce corrected data that resembles within acceptable limits the true input signals that would have been measured in vacuum by a perfect system. Corrupting effects include the atmosphere, electronics, physical hardware such as antennas and how they perform under varying observing conditions, and signal propagation effects such as solar and planetary gravitational deflection and even secular aberration.

This document presents the functional and operational requirements necessary to support calibration of the ngVLA telescope. These requirements shape aspects of the hardware, software, and operational elements of the ngVLA's design.

Section 5 presents system-level architecture-dependent Level 1.1 requirements and associated explanatory notes. The notes contain elaborations regarding the meaning, intent, and scope of the requirements. These notes form an *important part of the definition of the requirements* and should guide the verification process. The notes contain an explanation or an analysis of how the numeric vales of the requirements were derived. For brevity and clarity, each derivation typically only considers the most demanding scenario(s) under which the requirement of interest influences the system. Where numbers are not well substantiated, this is documented in the notes. In this way, the trade-space available is apparent to scientists and engineers who will guide the evolution of the ngVLA calibration strategy and overall system design.

Requirement IDs are static once assigned and therefore not always in sequential order due to subsequent revisions of the associated documents. Traceability is indicated for each requirement.

The requirements presented in this document have been developed by translating higher-level System Requirements [AD03] into performance requirements for the ngVLA system. This process has resulted in some requirements that are more demanding than can be delivered by the current ngVLA design. These differences will be addressed as the facility concept matures. This document informs the trade-space for potential future compromises between science performance, technical capabilities, project risk, and cost. If, however, the ngVLA can be delivered with better performance than required below, while remaining within cost limitations, then this should be considered.

5 L1.1 CALIBRATION REQUIREMENTS

This section presents system-level L1.1 requirements that are relevant to supporting calibration of the ngVLA. Broader context is provided by the material referenced in Section 2. The L1.1 requirements are implementation-specific in that they are calculated using numeric values for fundamental parameters such as antenna diameter, number of antennas, and maximum baseline length. General assumptions are presented in Section 5.1. Assumptions specific to particular requirements are stated in each case. The L1.1 requirements will need to be reassessed if assumed parameter values change significantly in the future.

Unless specified otherwise, parameter definitions in this document follow their usage in the System Requirements [AD03], many of which are inherited from the Science Requirements [AD01]. Traceability for each L1.1 requirement is shown to the relevant system-level requirements from AD03 and to other L1.1 requirements developed in this document.

Unless specified otherwise, the system can be assumed to be fully functioning, including mitigation for radio frequency interference (RFI), under the precision environmental conditions defined in AD06.

Calculations typically assume worst-case inputs so as to assess limiting performance. Accordingly, calculations involving image dynamic range assume a worst-case definition given by the ratio of peak surface brightness in the field relative to the rms noise of the source-free background. This is similar to the formal ngVLA definition from AD01, though the formal definition will result in larger measures of image dynamic range for some fields of view due to incoherent contributions in rms dynamic range floors from each contributing beam of surface brightness (e.g. consider calculations presented in RD03).

Requirements are grouped by the calibration quantity under consideration, rather than being aggregated by target subsystem. For example, the requirements presented for Antenna Pointing in Section 5.2.1 are of interest not only to the Antenna subsystem but also to the Computing subsystem.

To minimize potential misinterpretation, the requirements presented in this document are typically more verbose than would normally be encountered in formal systems engineering documentation.

5.1 Assumptions

Parameter	Value	References
Antenna	All antennas shall be alt-az mounted without third axis rotation (i.e. without dish rotators).	AD04
Feed Basis	All antennas shall be equipped with dual orthogonal linear feeds in all frequency bands.	AD04
Noise Diodes	One temperature-stabilized noise diode shall be installed per feed and antenna.	AD04
Independent Atmospheric Delay Calibration Subsystem	If required, all antennas can be equipped with an independent atmospheric delay calibration subsystem, for example incorporating 22 GHz water vapor radiometers.	AD04
Receiver RF Ranges	Band 1: 1.2 – 3.5 GHz Band 2: 3.5 – 12.3 GHz Band 3: 12.3 – 20.5 GHz Band 4: 20.5 – 34.0 GHz Band 5: 30.5 – 50.5 GHz Band 6: 70.0 – 116.0 GHz	FE0101–FE0106
IF Bandwidth	3.5 GHz, DS (RF $<$ 10.5 GHz) 3.5 GHz/SB, 2SB (10.5 – 50.5 GHz) 7 GHz/SB, 2SB (70 – 116 GHz)	IRD0301–IRD0306

Parameter	Value	References
Interferometric Sensitivity (Naturally-weighted continuum rms noise over RFI-free 1 GHz bandwidth for a single polarization and single baseline in 1 hour with 18 m apertures)	Band 1: 140 μJy/beam Band 2: 160 μJy/beam Band 3: 140 μJy/beam Band 4: 190 μJy/beam Band 5: 300 μJy/beam Band 6: 790 μJy/beam	AD04
Number of Antennas in Array	A notional array of 107×18 m antennas will be assumed when deriving L1.1 requirements related to the main array. L1.1 requirements related to the short baseline array will assume the full 19×6 m antennas in the reference array.	AD04, RD02
Self-Calibration	Requirements will be derived without allowing for potential benefits from self-calibration, unless stated otherwise, as easy application may not be possible in every standard observing scenario.	—

The ngVLA Reference Design [AD04] calls for alt-az antennas and linearly polarized feeds. The latter is to facilitate larger bandwidth ratios than circular feeds, though this is only strictly relevant for the lower frequency bands. Linear feeds are not necessarily required at the higher bands, though the choice removes the additional complication of requiring conversion between linear to circular polarization, which in turn reduces cost and improves performance (circular polarizers will slightly degrade sensitivity). Following the Reference Design, this document will assume the use of alt-az antennas. Given the significance of polarization feed basis to the overall facility design, Section 5.6 provides an independent and unbiased examination of feed basis selection from a calibration perspective. The outcome of this investigation is a robust justification for the choice of linearly polarized feeds. As a result, this document will assume the use of linearly polarized feeds in all bands.

Similarly, while the Reference Design [AD04] calls for the installation of an independent system for calibrating atmospheric delays over the array, for example using 22 GHz water vapor radiometers (WVRs), this document will only assume that this is an in-scope possibility. Given the significance of this decision, Section 5.3.1.1 provides an independent and unbiased examination of the motivation for installing an independent atmospheric delay calibration subsystem (IADCS).

The Front End (FE) requirements for the 6-band receiver design are from AD12. The Integrated Receiver and Downconverter (IRD) requirements are from AD13. Radio frequencies (RFs) below 10.5 GHz will be accessed using direct-sampled (DS) receivers while higher frequencies will be accessed using sideband-separating (2SB) receivers. Intermediate frequency (IF) bandwidths per sideband (SB) are indicated for the latter. Note that the band 2/3 transition at 10.5 GHz for the IRD modules does not coincide with those of the planned feed and cryogenic amplifier bands. Related system requirements are SYS0903, which requires the system to transmit and process a minimum of 14 GHz/pol from each antenna (with a goal of 20 GHz/pol), and SYS1401, which requires support for 0.1 km/s spectral resolution.

Interferometric sensitivities are from AD04, scaled to standardized values here. Equivalent sensitivities for 6 m apertures are obtained by multiplying by the inverse aperture area ratio, i.e. by factor $(18/6)^2 = 9$.

Several L1.1 requirements in the following sections are driven by the number of antennas in the array. The most demanding ngVLA science cases are expected to use most if not all antennas to achieve objectives of resolution and/or sensitivity. Imaging performance simulations [RD02] indicate that the bulk sensitivity resulting from tapering to achieve a nominated angular resolution scale will be provided by approximately half of the collecting area. The reference Main Array (MA) contains 214×18 m antennas [AD04] (equivalent to 0.05 km^2 collecting area). Therefore, the L1.1 requirements presented below for 18 m antennas will assume a notional array with 107×18 m antennas that span the same baseline range as the full MA. The reference Short Baseline Array (SBA) contains 19×6 m antennas [AD04]. This complete array will be assumed for all L1.1 requirements presented below for 6 m antennas. The reference Long Baseline Array (LBA) contributes an additional 30×18 m antennas to the ngVLA [AD04], though this explicit number of LBA antennas does not currently factor into any of the L1.1 requirements presented in this document.

The L1.1 requirements presented below have been developed without including potential benefits from self-calibration (direction independent or dependent). This is because it cannot be assumed that self-calibration can be used in all cases for ngVLA observations. For example, direction-independent gain self-calibration may be difficult for extended targets especially if they are not fully spatially sampled. Similarly, direction-dependent pointing self-calibration may be difficult for fields in which there is negligible off-axis emission.

5.2 Antenna Characteristics

Antenna requirements are presented below for Pointing, Surface Setting and Primary Beam, Feed Positioning, and Motion. See AD06 for definitions of Precision and Normal operating conditions.

5.2.1 Pointing

Parameter	Req. #	Value	Traceability
Antenna Pointing	CAL0201	2D radial errors (σ_2, mean of Rayleigh distribution) shall satisfy: 18 m Precision: $15''$ blind, $3''$ offset; 18 m Normal: $25''$ blind; $5''$ offset; 6 m Precision: $40''$ blind, $8''$ offset; 6 m Normal: $85''$ blind; $17''$ offset. Systematic pointing errors incurred over a 30 min time window including 3° slew to/from a target shall be within 70% of the offset values under precision conditions.	SYS6103, CAL0702, SYS6107, SYS6108, SYS1061
Spectral Line Noise Leakage (Arising From Pointing)	CAL0202	Calibration and imaging pipeline shall implement software and heuristics for estimating worst-case noise level leaked from strong spectral lines at different spatial locations due to limited pointing accuracy.	CAL0201, SYS6105, SYS6106

Antenna pointing will be affected by several slowly varying systematic terms such as imperfections of the antenna and the pad, gravitational forces, wind loading arising from the mean wind velocity, and thermal loading from the sun. Depending on the needs of the astronomical observation, these slowly varying effects can be removed by frequent offset pointing observations. In addition, there will also be random pointing errors arising from more rapidly varying effects such as wind gusts (about the mean wind velocity) and anomalous refraction. Random errors will also be present at some level due to the limited mechanical repeatability of antenna pointing, arising for example from solar orientation and thermal gradients.

Errors in antenna pointing will lead to amplitude and spectral index errors. Accurate pointing is important for high dynamic range observations and for mosaiced observations, particularly at the higher frequencies where the beam size is smaller. It is anticipated that a significant fraction of ngVLA observations will be mosaiced, perhaps 60% overall and involving all frequency bands [AD07].

When required, pointing calibration must be performed prior to astronomical observations or else the data will be corrupted. In general, pointing solutions cannot be interpolated backwards in time (this can be mitigated in some cases by performing pointing self-calibration [RD11], which requires emission to be present at locations throughout the primary beam). This makes pointing calibration critical for observations that require offset pointing. When needed, pointing solutions must be updated on a timescale that is short enough to over-sample all slowly-varying dynamic effects.

Requirement SYS6103 calls for 35 dB imaging dynamic range[1] over wide-field mosaics at 27 GHz. This can be translated to a pointing requirement by first considering the idealized relationship between dynamic range limit D for a Stokes image (e.g. Stokes I) and antenna-based amplitude errors ϵ (correlated for both polarizations on a given antenna) for an array comprising N antennas, given by RD03 as

$$D \approx \frac{N}{\epsilon} \ . \tag{1}$$

Next, by approximating the true profile of an antenna's primary beam (e.g. Airy disk or cosine-squared) with a Gaussian, the relationship between mean 2D radial pointing error σ_2 and antenna amplitude error ϵ resulting from observation of a source offset by angle θ from the field center can be estimated using

$$\epsilon \approx \exp\left[-4\alpha^2 \ln 2\right] - \exp\left[-4\left(\alpha + \kappa\beta\right)^2 \ln 2\right] \ , \tag{2}$$

where $\beta = \sigma_2/\mathrm{HPBW}$ is the fractional 2D error in units of primary beam half-power beam-width (HPBW), $\alpha = \theta/\mathrm{HPBW}$, and worst-case projection of a 2D pointing error onto θ over multiple sources of emission yields $\kappa \approx 1$. To be clear, σ_2 is the mean of a Rayleigh distribution arising from tracking with two assumed independent axes, each characterized in 1D by zero-mean and normally distributed tracking error σ. For example, for drive motions in elevation X and azimuth Y with respective 1D errors given by σ_X and σ_Y, and assuming that any systematic pointing offsets in X and Y have been removed through pointing calibration such that $\langle X \rangle = \langle Y \rangle = 0$ (offset pointing) or that this condition is satisfied without pointing calibration over long timescales (blind pointing), the residual 2D tracking offset is described by $\rho = \sqrt{X^2 + Y^2}$ with $\sigma_X = \sigma_Y = \sigma$ and the mean 2D radial pointing error is $\sigma_2 \equiv \langle \rho \rangle = \sigma\sqrt{\pi/2}$. See RD46 for verification of these equations using simulations.

These relationships indicate that to achieve 35 dB dynamic range at the center of a single pointing with $N = 107$, the induced amplitude errors must be less than 3% and pointing errors must satisfy $\beta < 1/9$. This translates to $\sigma_2 = 14''$ with 18 m dishes at 27 GHz (center of band 4). Performing this exercise using the 45 dB on-axis requirement at 8 GHz (SYS6103) leads to a less strenuous requirement of $\sigma_2 = 15''$. However, pointing errors are more pronounced off-axis. For pointing error $\beta = 1/9$, the amplitude errors

[1] Note that the anticipated continuum sensivity of the ngVLA using $N = 107$ antennas will be sufficient to deliver 35 dB dynamic range in 1 hour on unresolved sources as faint as 5 mJy in band 6 and 1 mJy in band 4 [AD04].

per antenna resulting from a point source located at the nominal primary beam -0.1 dB, -2 dB, and -12 dB contours (radial offsets HPBW/10, $\mathrm{HPBW}/\sqrt{6}$, and HPBW) will range between approximately 9%, to 16%, and 3%, respectively. These errors will be important when imaging extended sources, reconstructing spectral indices, and attempting high dynamic range imaging of single-pointing fields if there are strong sources located off-axis. They will also be important for mosaiced observations.

For a hexagonal mosaic with pointing separation $\mathrm{HPBW}/\sqrt{2}$ (typical widest separation sufficient to obtain approximately uniform mosaic sensitivity), and assuming that each contributing primary beam is only imaged out to the HPBW (imaging further provides negligible sensitivity gain), the worst-case amplitude error in the mosaic will be located equidistant from 3 contributing pointings at their overlapping -2 dB primary beam contours. For $\beta = 1/9$ with $N = 107$, the dynamic range limit in a single pointing that contains a point source located at the -2 dB contour is 28 dB. Thus, the dynamic range range limit in a mosaic with $\mathrm{HPBW}/\sqrt{2}$ beam throw could be as low as 31 dB (i.e. factor $\sqrt{3}$ improvement), despite the 35 dB dynamic range limit expected at the center of each individual pointing. (Note that this calculation assumes that pointing errors from contributing pointings are statistically independent. This is likely to be approximately true because a common source would sample different locations in each antenna's primary beam in each pointing.) Therefore, in order to satisfy 35 dB at 27 GHz over a wide-field mosaic, pointing errors must instead satisfy $\beta < 1/25$, yielding a more stringent requirement of $\sigma_2 = 5''$ for 18 m dishes.

However, this too is insufficient for ngVLA. While $\sigma_2 = 6''$ satisfies SYS6103, it is insufficient for maintaining pointing to within a minimum acceptable constraint of $\beta < 1/10$ at the highest observing frequency in band 6. This translates to $\sigma_2 = 3''$ at 116 GHz and sets the ngVLA 18 m requirement for pointing accuracy under the most favourable observing conditions.

For reference, Table 1 presents dynamic range limitations for snapshot imaging scenarios in which a single point source is located at the center of a single pointing, D_1, at the -2 dB primary beam contour in a single pointing, D_2, and at the overlapping -2 dB contours in a hexagonal mosaic (described above), D_3, for frequencies f specified at band edges in the current 6 band design. The estimates assume an array with 107 antennas, precision offset pointing accuracy $\sigma_2 = 3''$, no other errors, and no self-calibration. Note that the D_2 and D_3 values represent approximately worst-case dynamic range limits for single pointing and mosaiced images, in which the brightest source in the visibility data is located near a pointing's -2 dB primary beam contour.

f (GHz)	D_1 (dB)	D_2 (dB)	D_3 (dB)
1.2	75	49	51
3.5	66	44	46
12.3	55	38	41
20.5	51	36	39
34	46	34	36
50.5	43	32	35
70	40	31	33
116	36	29	31

Table 1 Dynamic range limits arising from 3$''$ precision offset pointing with 107×18 m dishes, $M=1$.

These limits may be improved in certain cases, for example by performing on-the-fly observations to scan over the vicinity of a strong source while sampling as many different primary beam locations as possible (i.e. attempting to 'average out' the pointing error for each antenna), or by employing pointing self-calibration if there is sufficient signal-to-noise within the primary beam to obtain pointing solutions on sufficiently short timescales to sample the true pointing variability. Heuristics will need to be developed to identify appropriate observing and pointing conditions for every proposed observation, including the option to employ pointing self-calibration in post-processing when it is likely to be beneficial.

Importantly, it should also be noted that for continuous observations that effectively comprise M statistically-independent snapshots (where M depends on the dynamical timescale of antenna pointing variations as well as the timescale for rotation of each baseline), Equation 1 will be improved by factor $\sqrt{M}$ [RD03]. This could lead to improvement beyond the values derived above, possibly by an order of magnitude or more in dynamic range over the course of a few hour observation. The benefit from $\sqrt{M}$ is neglected in the calculations presented earlier for two key reasons. First, this is in order to derive robust worst-case pointing requirements that will support high dynamic range from short observations. This is strongly motivated by the needs of calibration (see CAL0702). And second, it is possible that wind-induced pointing errors will be correlated over short baselines (perhaps up to a few hundred meters). This would effectively lower the factor of N assumed above and in turn reduce the snapshot image dynamic range performance. $M=1$ is therefore assumed to offset this potential reduction over an extended observation.

Antenna pointing errors can be separated into repeatable systematic errors (i.e. statistical accuracy, requiring offset pointing corrections to account for slowly-varying systematic effects) and non-repeatable statistical errors (i.e. statistical precision). There are 4 states for which pointing requirements are needed, spanning the matrix of normal and precision operating conditions, and blind and offset pointing modes. The precision offset pointing requirement is defined by requiring that SYS6103 will be satisfied under precision operating conditions and ensuring that $\beta<1/10$ at 116 GHz; as described earlier, this requires $\sigma_2=3''$ with 18 m dishes. The normal offset pointing requirement is driven by the desire to support 35 dB dynamic range over a mosaic at 27 GHz without requiring precision conditions; as described earlier, this requires $\sigma_2 = 5''$. To obtain good offset pointing solutions, historical analogues (including the VLA) suggest that systematic pointing errors cannot be larger than approximately 5 times the statistical pointing errors. Note that this is only applicable at frequencies where the statistical and systematic pointing errors are not substantial fractions of the primary beam width. For example, consider performing offset pointing in band 5, where the HPBW is $70''$ for an 18 m dish at the upper frequency bound at 50.5 GHz. The normal offset pointing requirement of $5''$ is then approaching HPBW/10. This should be sufficient to obtain good pointing solutions. This also suggests that it will not be appropriate to calculate offset pointing corrections using band 6 in normal observing conditions. However, assuming factor 5, if the systematic pointing error is $25''$, this is a excessive fraction of the $35''$ half-power half-width, indicating that band 4 is preferred for calculating offset pointing corrections in normal conditions. Assuming factor 5, the blind pointing requirements are $\sigma_2 = 15''$ in precision conditions and $\sigma_2 = 25''$ in normal conditions. These requirements have implications for array scheduling. For comparison with Table 1, Table 2 presents 'worst-case' dynamic range limits arising from normal blind pointing with accuracy $\sigma_2 = 25''$.

f (GHz)	D_1 (dB)	D_2 (dB)	D_3 (dB)
1.2	57	39	42
3.5	48	35	37
12.3	37	29	32
20.5	33	27	30
34	28	25	28
50.5	25	24	26
70	23	23	25
116	21	22	24

Table 2 Dynamic range limits arising from $25''$ normal blind pointing with 107×18 m dishes, $M = 1$.

The 19×6 m antennas that make up the short baseline array must also satisfy the 35 dB requirement for mosaic dynamic range at 27 GHz (SYS6103). Performing a calculation similar to that presented above, but now including an additional improvement factor $\sqrt{M}$ with $M = 10$, yields a requirement of $\sigma_2 = 8''$ under precision conditions. This value of M can be obtained, for example, if dynamic wind loading produces statistically independent pointing errors on timescales no slower than 30 sec over the course of a 5 min observation. While the use of $M > 1$ differs from the 18 m calculations presented above, it is suitable here because calibrator suitability tests (CAL0702) will likely be driven by the 18 m array, therefore reducing the need for ultra-rapid high dynamic range imaging when using the 6 m array. Offset pointing with $\sigma_2 = 8''$ also satisfies the minimum acceptable constraint of $\beta < 1/10$ at 116 GHz.

The 6 m normal offset pointing requirement is driven by the desire to support a 35 dB dynamic range on-axis at 27 GHz with $M = 1$. This requires $\sigma_2 = 17''$. Following the factor 5 between offset and blind pointing described earlier, this requires precision blind pointing error $\sigma_2 = 40''$ and normal blind pointing error $\sigma_2 = 85''$. Tables 3 and 4 presents dynamic range limits arising from precision offset and normal blind pointing errors, respectively.

A minimum timescale of 30 min is placed on the offset pointing requirements during which systematic antenna deformations (e.g. arising from changes in temperature or wind loading) must not cause the pointing vector to systematically veer beyond 70% of the specified offset limits. The factor of 70% is selected so that the quadrature sum of systematic and statistical errors is within 20% of the statistical value alone. The timescale of 30 min is derived by seeking minimum 80% time on target, approaching the goal of 90% from SYS1061, with typical 2.5 min pointing calibration duration and worst-case 30 sec calibrator referencing every 5 min. The offset requirements must also be satisfied within this time window over a maximum 3° slew. This is necessary to support gain calibration for which the antennas must repeatedly slew between a science target and adjacent calibrator. A maximum angle of 3° will facilitate gain calibration up to and including band 6 (see Section 5.2.4).

f (GHz)	D_1 (dB)	D_2 (dB)	D_3 (dB)
1.2	69	42	44
3.5	60	37	39
12.3	49	31	34
20.5	44	29	32
34	40	27	29
50.5	37	25	28
70	34	24	26
116	29	22	24

Table 3 Dynamic range limits arising from 8″ precision offset pointing with 19×6 m dishes, $M = 1$.

f (GHz)	D_1 (dB)	D_2 (dB)	D_3 (dB)
1.2	48	31	34
3.5	39	27	29
12.3	28	21	24
20.5	24	19	22
34	20	17	20
50.5	17	16	18
70	15	15	17
116	13	15	16

Table 4 Dynamic range limits arising from 85″ normal blind pointing with 19×6 m dishes, $M = 1$.

The pointing error simulations presented by RD46 indicate that $\beta < 1/13$ is required to yield image fidelity > 0.95. This is satisfied by the $3''$ offset pointing requirement for 18 m dishes up to 116 GHz and by the $8''$ offset pointing requirement for 6 m dishes up to 100 GHz. Note that RD46 uses a slightly different definition of image fidelity to that adopted by AD01 for the ngVLA project (to optimize compatibility with the carefully designed simulations) and that SYS6107 (also SYS6108) calls for an image fidelity goal of 0.9. Therefore, conservatively accounting for the slight difference in definitions, the 6 m and 18 m pointing requirements above satisfy SYS6107 over the full ngVLA frequency range. See RD44 for alternate definitions of image fidelity.

Finally, requirements SYS6106 and SYS6105 call for 50 dB emissive and 40 dB absorptive spectral dynamic ranges, respectively. For observations in which only a single spatial position exhibits a strong spectral line in emission, 50 dB spectral dynamic range can be facilitated without requiring the imaging dynamic range limit to be anywhere near 50 dB. However, it is possible that multiple spatial locations in a cube could exhibit a 50 dB spectral line with respect to the nominal channel noise level, where the spectral lines may peak in different channels. At 50 GHz, with 107×18 m dishes under the most favourable precision offset observing conditions with $\sigma_2 = 3''$, the per-channel image dynamic range limits will be 43 dB if sources are confined to the center of a single pointing, 32 dB if sources are located at the -2 dB primary beam contour in a single pointing, and 35 dB if sources are located at the overlapping -2 dB contour in a hexagonal mosaic (following details presented above). Taking an example in which two spectral lines are detected at the 0 dB (on-axis) and -2 dB contours in a single pointing, with each detected at a different frequency, then the spectral dynamic range in the on-axis spectrum will be limited to 32 dB (rather than 43 dB) when taking the ratio between the line peak and the noise level in the channel corresponding to the line peak of the off-axis source. The dynamic range will still remain 50 dB when taking the ratio between the line peak and other channels. Thus a form of noise leakage will occur in which bright spectral features in one spatial source will affect the spectra of other spatial sources. Heuristics will need to be developed to identify these situations and to estimate the impact on spectra throughout a single pointing or mosaiced cube. Note that the benefit from $\sqrt{M}$ described earlier will certainly minimize this effect. However, some contamination may still occur, and it is highly likely that an investigator interested in detecting faint spectral lines at 50 dB would also be interested in knowing where in the cube potential spurious detections might be located, even if the amplitude of these effects may be uncertain within some factor. The same heuristics may be useful for identifying emission lines that could potentially contaminate absorption lines.

5.2.2 Primary Beam and Surface Setting

Parameter	Req. #	Value	Traceability
Primary Beam Model Accuracy	CAL0203	The power pattern for each polarization on each 18 m antenna shall be measured to a repeatable accuracy of better than 1% of the boresight response and within phase error $0.3°$, at all points within the -10 dB power contour (-5 dB voltage contour), within a 10 MHz bandwidth over at least 10 spot frequencies spanning the band. This means that at the -10 dB power point the accuracy of a power measurement is 10%. These power patterns shall be measured at different parallactic angles, elevation angles, offset pointing orientations, and sampled with sufficient frequency resolution to enable a global model to be developed per band, antenna, and polarization. The values above are requirements for band 2 and goals for all other bands. The required accuracies for band 4 are 10% and $3°$. The requirements for 6 m antennas are 1% and $0.3°$ in band 4; these are goals in all other bands. Best achievable accuracies beyond -10 dB are desired.	SYS1901, SYS6103, SYS6104
Antenna Aperture Plane Error	CAL0204	Aperture plane errors (double the values of the primary and secondary surface errors combined including any systematic antenna deformations) for 6 m and 18 m dishes shall satisfy: Precision: $340\,\mu$m rms, Normal: $800\,\mu$m rms.	SYS6103
Antenna Error Scatter Pattern	CAL0208	Equation 4 shall be satisfied on-axis.	SYS6103

Errors in the assumed model of the primary beam will lead to spectral index errors and dynamic range limitations in single pointing and mosaiced observations. Surface errors will scatter power from the main beam into the sidelobes, reducing the surface efficiency and limiting dynamic range. Surface errors can be thought of as leading to statistical errors about the systematic assumed primary beam model.

Visibility errors will arise from errors in the assumed primary beam model (see A-projection terms in the numerator sum in Equation 7 from RD12). To satisfy 45 dB image dynamic range at 8 GHz (SYS6103), the 18 m antenna power (proportional to voltage squared) pattern for each polarization needs to be known to better than 1% per channel over at least 10 statistically independent channels. This assumes the frequency dependence of the primary beam can be effectively described by a scaled frequency-independent model (suitable for the unblocked aperture design under consideration for ngVLA). This requirement needs to apply out to the point in the beam where the power response is 10% of the peak (or ideally 1%), so as to support high dynamic range imaging for single pointing observations and mosaiced observations. This requirement is calculated by considering Equation 1 with $N = 107$ and with the additional improvement factor $\sqrt{2N_c}$ [RD03], accounting for N_c statistically independent channels in which a primary beam is measured per polarization. The bandwidth of each channel should be no larger than ~ 10 MHz to prevent contamination by wide-band effects. Note that, conservatively, any benefits from parallactic angle rotation and baseline rotation are ignored in this calculation so that worst-case limits are derived (i.e. factor $\sqrt{M}$ is not used; e.g. consider a short observation, or a long observation of a field containing significant extended emission such that beam rotation with parallactic angle yields negligible improvement). If the requirement for power pattern accuracy is 1% of the boresight power response, the corresponding requirement on phase errors is half this [RD03], namely $0.3°$. These values are 10% and $3°$, respectively, if calculated for 35 dB at 27 GHz. These levels of accuracy are not expected to be problematic. Efforts should be made to sample the power patterns at different elevation angles and with sufficient frequency resolution to enable a global model to be developed per antenna. Effort should also be dedicated to testing the impact (if any) of systematic dish deformations associated with offset pointing, and to assessing requirements for primary beam accuracy in far-out sidelobes. It is not anticipated that any real-time sensing of antenna deformation, nor associated post-processing, will be required.

A 40 dB source will be required to measure the primary beam to the accuracies above, at all raster positions sampling the full aperture plane, within channel bandwidths no wider that 10 MHz. Assuming a 1 Jy source, this can be attained within 1.5 min integration time. It will therefore be feasible to perform this measurement over a large number of raster positions (and similar measurements over all bands) within a realistic timeframe. Such measurements should be performed upon antenna construction, then periodically during commissioning to validate stability and inform requirements for future sampling frequency (potentially many years). Primary beam measurements to achieve 35 dB image dynamic range at 27 GHz are less demanding, and therefore also attainable using a celestial source.

Accuracy in the primary beam model is also relevant for SYS1901 and SYS6104, which require 0.03% on-axis post-calibration residual linear polarization leakage and 0.3% off-axis. The residual leakage off-axis will effectively arise from the quadrature sum of the residual leakage on-axis (examined in Section 5.6.3) and the primary beam model accuracy [e.g. RD42]. The latter is given by at worst 0.03% (35 dB at 27 GHz, or equivalently 10% averaged over 10 channels, 2 polarizations, and 107 antennas, as above). Their quadrature sum is within the required 0.3% off-axis.

The relevant requirement for the 6 m antennas is 35 dB at 27 GHz (the 45 dB requirements at 8 GHz is for on-axis deep fields that do not focus on recovering extended emission). Following the calculation above, but with $N = 19$, the requirement for 6 m antenna power pattern accuracy is 1% of the boresight power response with a corresponding requirement on phase errors given by $0.3°$.

Surface errors must be minimized in order to maximize the forward gain of an antenna and limit amplitude errors arising from the antenna scatter response. The surface efficiency is given by Ruze [RD04] as

$$\eta_{\rm sf} = \exp\left[-\left(\frac{2\pi\sigma_{ap}}{\lambda}\right)^2\right], \quad (3)$$

where σ_{ap} is the path length error in the aperture plane given by $\sigma_{ap} = 2\sigma_{sc}$ where σ_{sc} is the rms error for the primary and secondary reflector surfaces combined including systematic geometric errors (antenna deformations). An aperture plane error of 340 μm is required to deliver no worse than -3 dB loss at 116 GHz (i.e. $\sigma_{sc} = \lambda/15.1$). The equivalent aperture plane error at 50 GHz is 800 μm. Losses within -3 dB are preferred to minimize complexity in A-projection models.

More restrictive values of σ_{sc} (and in turn σ_{ap}) may be required to offset the presence of correlated surface errors. For reflector diameter D with errors correlated over distances D/R (e.g. due to panel setting errors, or setting errors in the backing structure fixture points that support a single-piece mold surface), a scatter pattern will be produced that is R times broader than the diffraction-limited main lobe [RD04, RD05]. Antenna surfaces with larger number of R segments will exhibit larger and less symmetric near-in sidelobes which must be compensated using a more restrictive surface error requirement.

To satisfy SYS6103 following a similar argument as for primary beam model accuracy above, the error scatter response $E(\theta)$ on-axis[2] (where $\theta = 0$) must satisfy

$$E(\theta = 0) < 10\log_{10}\left(\frac{N_{\rm ant,indep}}{D}\right), \quad (4)$$

where $N_{\rm ant,indep}$ is the number of antennas with statistically independent surface errors (up to 107 for 18 m dishes, up to 19 for 6 m dishes) and D is the dynamic range requirement (45 dB for 18 m dishes at 8 GHz, 35 dB for 6 m dishes at 27 GHz). Note that to satisfy this equation, smaller surface errors than specified by CAL0204 may be required. Note also that, as earlier for primary beam model accuracy, there is no factor of $\sqrt{M}$ in Equation 4 so that worst-case limits are derived. The error scatter response in the equation above represents a band average. In the most extreme case $N_{\rm ant,indep} = 1$

[2] For simplicity, Equation 4 assumes that the off-axis scatter response is approximately the same as the on-axis response. In reality the off-axis response will be lower, but this difference is unlikely to be significant until beyond the HPBW.

and $E(\theta = 0) < -45$ dB, for example if all antennas are cast from the same full-surface mold, attached to infinitely rigid backup structures, transported to each station without deformation, and mounted identically. In the opposite extreme, if $N_{\text{ant,indep}} = 107$, then the requirement is $E(\theta = 0) < -25$ dB. A requirement for error scatter response therefore depends on the choice of antenna design. If Equation 4 is satisfied, then the error scatter response will not dominate pointing or primary beam model errors.

5.2.3 Feed Positioning

Parameter	Req. #	Value	Traceability
Feed Setting Calibration Residual	CAL0205	Positioner errors shall distort the primary beam power pattern per polarization by no more than 0.3% of the boresight response and $< 0.1^\circ$ phase at any position within the -10 dB power response for 18 m antennas at 8 GHz and for 6 m antennas at 27 GHz. These are goals at other band centers. The requirements are 3% and $< 1^\circ$ respectively for 18 m antennas at 27 GHz.	CAL0203, SYS6102
Band Switching	CAL0206	18 m antennas shall be capable of switching between frequency bands 1 and 2 (goal: others) within 7 sec including settling time, with ability to cycle bands every 5 min.	CAL0303, CAL0207, SYS0908

The current ngVLA antenna designs for the 6 m and 18 m dishes incorporate a fixed subreflector and a motorized adjustable feed positioner (X-Y plane). Accurate setting of the feed positioner is required to prevent loss in efficiency and primary beam abnormalities.

Errors in feed positioning will lead to systematic distortions in primary beam power and phase patterns. To ensure that these distortions remain within the error budget calculated for CAL0203 after combining 10 channels, variations in the power and phase patterns arising from positioner errors must be kept to within 0.3% of the boresight power response and 0.1° for each polarization on each antenna at the center band frequencies of 8 GHz for 18 m antennas and 27 GHz for 6 m antennas, following CAL0203. The respective errors are required to be within 3% and 1° at 27 GHz with 18 m antennas. If total errors are approximated by adding the systematic and statistical errors in quadrature, this requirement will ensure that feed positioner errors contribute no more than 40% to the primary beam error budget.

Note that feed positioning errors are also relevant for in-beam calibration. SYS6102 requires relative astrometric accuracy $< 1\%$ of the synthesized beam FWHM for a bright $(\mathrm{SNR} > 100)$ point source (this requirement is discussed further in Section 5.3.2). Phase differences between two points within the -10 dB primary beam must therefore be kept within $0.01 \times 360° = 3.6°$. Assuming worst-case feed positioning errors that lead to correlated primary beam errors between polarizations, there are N statistically independent primary beams over the array. Thus for $N = 107$, the requirement is that any phase gradient per antenna polarization arising from a feed positioning error must be less than $35°$. This is satisfied by the much stricter requirement above.

RD13 presents equations to convert between positioner error and efficiency loss. To satisfy CAL0205, a similar model will need to be developed to convert between feed setting errors in physical units and the primary beam distortions examined above.

CAL0206 is motivated by CAL0303 and CAL0207. See discussion for CAL0303 in Section 5.3.1.2.

5.2.4 Motion

Parameter	Req. #	Value	Traceability
Antenna Motion	CAL0207	6 m and 18 m antennas shall be capable of slewing $3°$ in 7 sec in precision conditions, including time to settle within offset pointing error	SYS1061

In order to calibrate fluctuations in atmospheric delay (described in more detail in Section 5.3.1), the antennas must be capable of repeatedly switching between a science target and nearby calibrator, transferring the atmospheric delay on the calibrator to the science target within a cycle time that is short compared to the atmospheric stability timescale. This demands fast slew and settle rates to maximize observing efficiency (time on science target). Antennas with fast slew rates are also needed to minimize time spent slewing between widely separated sources, minimize time spent performing offset pointing calibration (slew to calibrator, raster scan, return), and to enable rapid cancellation of atmospheric fluctuations when observing in total power mode (slew across extended source).

While there are technical solutions for maximizing time between calibrator scans (such as water vapor radiometry, addressed later in this document), which will in turn minimize required slew rates without sacrificing observing efficiency, the fast switching approach must remain feasible and part of ngVLA design in order to minimize overall project risk. Assessment of the fast switching approach therefore drives this anntena motion requirement, regardless of the technique that will be ultimately implemented for calibrating fluctuations in atmospheric delay.

The most demanding requirement for antenna motion arises from considering slew rates for gain calibration at the highest frequencies, where radio source counts are lower and angles to suitable nearby calibrators are larger. In an early design study, RD06 concluded that a 1 minute cycle time between science target and calibrator should be sufficient to correct for atmospheric delay in band 6 at night throughout most of the year. RD06 also found that a suitable calibrator with minimum required 3 sec integration time should be available within 2° of any position in the sky. This observing strategy is incompatible with SYS1061, which states a goal for observing efficiency greater than 90% in standard observing modes. However, for the sake of deriving a risk-mitigating antenna motion requirement, it is justified to consider fast switching that delivers lower observing efficiency. Assuming a 1 minute switching timescale and 6 sec integration time on the calibrator (double 3 sec because RD06 assumes $N = 200$ antennas rather than $N = 107$), 70% efficiency can be obtained by requiring that antennas are capable of slewing 3° and settling at the new desired pointing location within 7 sec. This requirement must be satisfied under precision conditions, suitable for observing in the highest frequency band.

5.3 Delay

The ngVLA is envisaged to operate as a quasi-connected-element[3] interferometer, including over continental scale baselines, with correlation taking place in near real-time. Delays must be calculated or measured to account for several contributions, including the atmosphere (neutral and ionized), source position, earth orientation, station locations, antenna structure, and electronics.

There is an additional fluctuating portion of delay due to the atmosphere, antenna, and electronics. Delay fluctuations limit resolution, limit the dynamic range of images, introduce artifacts, and reduce sensitivity by decorrelation. Without effective calibration of these fluctuations, the maximum usable baseline (exhibiting say $> 90\%$ coherence) at 116 GHz would be only 400 m [RD07 Equation 13.118].

The title of this section "delay" implicitly indicates requirements for both delay and phase. A delay τ will produce a change in signal phase $\Delta\phi$ that is proportional to frequency ν. Alternatively, all frequencies in a bandpass range can be shifted by the same phase if the local oscillator experiences a phase shift.

Delay can be specified in units of path length and time. These are connected by the speed of light $c \approx 300\,\mathrm{nm/fs}$ and can be used interchangeably. The corresponding fractional phase change is given by $\Delta\phi/(2\pi) = \tau_{\mathrm{path}}/\lambda = \tau_{\mathrm{time}}\nu$. At 116 GHz, a phase change of 1 deg corresponds to a delay of 24 fs.

The requirements presented below refer to antenna-based delays. This document will assume uncorrelated variations in antenna-based delays, in which case the resulting baseline-based delays will be $\sqrt{2}$ larger. If this condition will not be met in practice, then the calculations below will need to be re-evaluated.

[3] It is anticipated that multiple masers will be required over the array, with a single maser supplying antennas within the central ~ 300 km and others supplying more distant antennas [AD04].

Furthermore, the requirements presented below are separated into delay drift (accuracy) and delay noise (precision), reflecting the systematic and stochastic components of delay, respectively. The drift component includes fluctuations that do not integrate down with time in the way that white noise would. The timescale for differentiating between these components is defined where appropriate in the sections below. The delay requirements below imply measurement and application with residuals within the specified values. The drift component may refer to residuals after a trend has been removed (e.g. subtract linear trend between scans on an astronomical calibrator), or in some cases (e.g. electronics) refer to deviations from common-mode drift. None of the drift requirements below refer to absolute drift.

5.3.1 Atmosphere

Parameter	Req. #	Value	Traceability
Atmospheric Delay Calibration Residual	CAL0303	Residuals shall satisfy: *Neutral:* 0.1 ps drift over 5 min, 1 ps noise rms in 8 sec with maximum 8 sec sampling rate (goal: 180 fs per 1 sec sampling rate); *Ionized:* $2/\nu^2$ ps drift over 5 min, $20/\nu^2$ ps noise rms in 10 sec, where ν is in units of GHz. The drift requirements are for motions over 3° on the sky. The ionized values are only goals for 6 m antennas.	SYS1061, SYS1502, SYS6103, CAL0207, CAL0403
Tropospheric Delay Measurement Capability	CAL0304	An independent tropospheric delay monitoring and calibration subsystem shall be installed on all 244×18 m antennas, and on at least 2×6 m antennas.	CAL0303
Amplitude and Phase Coherence Over Multiple Observations	CAL0305	The observatory scheduling process and data reduction pipeline shall be capable of executing an observing strategy and processing the resulting data in which the flux density scales and positional (phase) reference frames are aligned over multi-epoch observations.	SYS6103

Parameter	Req. #	Value	Traceability
Ionospheric Delay Measurement	CAL0306	The pipeline shall be capable of measuring and correcting for ionospheric delay fluctuations using frequency-switched (where required) band 1 observations of a phase calibrator located on-axis. Goal is to achieve this over an arbitrary field in which the brightest source may not be located on-axis. The scheduler shall ensure sufficient time on calibrator to achieve the necessary solution accuracy from CAL0303.	CAL0303
Ionospheric Disturbance Monitoring	CAL0307	The scheduler shall ingest and utilize a real-time spatio-temporal map of ionospheric disturbances on ~ 5 min timescales over the array.	CAL0303, SYS2501
Proposal Content: Estimated Dynamic Range	CAL0308	Proposals for ngVLA observing time shall specify the required image dynamic range.	CAL0303, SYS2601
Scheduler Start/Stop/Restart	CAL0309	The scheduler shall be designed to make informed decisions about scheduling and early termination of observing blocks based on weather conditions, and to account for previously stopped observations in the ranking process.	CAL0308, SYS2601
Interplanetary Medium Monitoring	CAL0310	The scheduler shall ingest and utilize real-time estimates of conditions in the interplanetary medium to avoid observing certain projects too close to the Sun.	CAL0303, SYS2501

Radio waves from an astronomical source must pass through intergalactic, interstellar, interplanetary, and terrestrial atmospheric media. The neutral and ionized components of these media will each produce a delay relative to propagation in vacuum. However, it is only in the immediate vicinity of the Earth that ray paths propagating toward Earth-based antennas will exhibit an appreciable difference in their delays. These differential delays will perturb the wavefront, causing decorrelation and leading to a degradation in dynamic range. Differential delays must be compensated to minimize these effects.

The image dynamic range limit for uncorrelated antenna-based phase errors ϕ is given by [RD03]

$$D \approx \frac{N\sqrt{M}}{2\phi}\,, \tag{5}$$

where the factor M represents the number of statistically independent successive snapshots in an observation. In the present context, M is related to the atmospheric coherence time over which phase fluctuations remain below a nominated threshold. Requirement SYS6103 calls for 45 dB imaging dynamic range at 8 GHz and 35 dB at 27 GHz. While both are relevant for 18 m antennas in the MA, only the former drives calculations below. Only the 35 dB requirement is relevant for 6 m antennas in the SBA.

Phase fluctuations in the neutral atmosphere are predominantly caused by temporal variations in tropospheric water vapor (dry atmospheric gases also contribute, as do ice particles when present). Phase fluctuations in the ionized atmosphere are mostly caused by variations in total electron content in the ionosphere. These neutral and ionized contributions to atmospheric delay are examined in turn below.

5.3.1.1 Troposphere

Radio waves propagating through the Earth's neutral atmosphere are most affected by the troposphere, located below altitudes of approximately 10 km, and in particular by water vapor that is poorly mixed in the troposphere. Tropospheric phase fluctuations can be treated as turbulent eddies that remain fixed as the atmospheric layer advects over the ground at a characteristic velocity aloft.

RD14 examined statistics of tropospheric phase fluctuations at the VLA during best-case observing conditions in winter and worst-case conditions in summer. RD14 inferred from these data, together with worldwide water vapor statistics, a general equation that conservatively predicts the growth of rms phase fluctuations on a baseline over time that is independent of baseline length, time of day, time of year, and geographic location (including altitude). This equation is relevant to ngVLA where the size and geographic distribution of the array implies that subsets of antennas will concurrently experience different atmospheric conditions. Using the rms phase growth relationship, RD14 assessed several phase calibration strategies for their capacity to support a 45 dB image dynamic range requirement. The phase calibration strategies examined were fast switching (rapid transfer of phase solutions from nearby calibrator to target), paired array calibration (where a subset of antennas view a nearby calibrator while the others view the target), self-calibration (using a bright unresolved source in the field of view), simultaneous multi-frequency observations (effectively self-calibration but utilizing an in-beam source that is brighter in a lower frequency band), and radiometric phase correction (e.g. using the 22 GHz water line, see RD07 Sec 13.3.2). RD14 found that at 8 GHz, tropospheric phase fluctuations must be tracked with approximately 10 sec cadence in order to attain 45 dB image dynamic range from a 3.5 hour observation on-target (i.e. $M = 1260$) with $N = 107$ antennas. The corresponding antenna-based phase error in Equation 5 is $\phi < 3°$. An observation length of 3.5 hours on-target (not including calibrator overheads) is selected for two reasons. First, this is the approximate timescale over which the anticipated continuum sensitivity of the ngVLA at 8 GHz [AD04] with $N = 107$ is expected to yield 45 dB image dynamic range for an unresolved source with flux density ~ 7 mJy. And second, as derived in RD14, 3 mJy is the approximate flux density threshold at which the noise within a 10 second self-calibration solution will induce phase errors in Equation 5 that exceed the threshold necessary to achieve 45 dB dynamic range (i.e. self-calibration will not be suitable with unresolved sources fainter than ~ 7 mJy). RD14 conclude that the only practical calibration strategy capable of sampling phase fluctuations on 10 sec timescales and in turn supporting a 45 dB image dynamic range requirement is water vapor radiometry (i.e. an independent atmospheric delay calibration subsystem is required). To achieve similar performance using fast switching on the most optimistic 10 sec calibration timescale would require sacrificing observing efficiency and would in turn lead to longer observing blocks to satisfy time on target. Additionally, RD14 conclude that a radiometer should ideally be placed on every 18 m antenna in the Main Array, even though tropospheric phase fluctuations on 10 sec timescales will be independent over ~ 100 m distances. This length scale is comparable with, though slightly larger than, the shortest anticipated baseline length of 30 m between any of the 18 m antennas. While placement of an independent WVR on every antenna will slightly increase hardware cost, it will likely reduce total costs through reduced project complexity (antenna designs, performance, and maintenance will be uniform, and overheads for optimizing dynamic scheduling to ensure there is at least one WVR-equipped antenna per grouping of adjacent antennas will not be required). For demonstration, the following material will accept WVR as a component of any implemented IADCS, though note that the requirements defined above do not explicitly force this particular solution.

The argument above does not necessarily extend to the 30×18 m LBA antennas. It is possible that other delay calibration strategies (e.g. paired antennas within individual LBA stations) may be sufficient to maintain coherence necessary for VLB science (currently there are no formal ngVLA science requirements for VLB image dynamic range). For now, the requirement is to equip VLB antennas with WVRs as this minimizes overall project complexity costs (e.g. uniform 18 m antenna design over ngVLA) and ensures that a consistent delay calibration strategy is available at each LBA station. (In the current Rev C antenna layout, one third of LBA antennas are located more than 500 m from another antenna, up to a maximum baseline of 1.7 km; these may present challenges for maintaining coherence in band 6.) Future work is needed to fully assess the costs/benefits of installing WVRs on VLB antennas.

Using Equation 6 from RD14 with $N = 107$ and 10 sec calibration timescale over 3.5 hours on-target ($M = 1260$), the image dynamic range limit as a function of frequency ν in GHz arising from tropospheric phase fluctuations, independent of weather conditions (short of observing through thunderstorms), is predicted to be

$$D_{tropo,MA} \approx \frac{10^{5.4}}{\nu} \quad . \tag{6}$$

Antenna-based phase errors $\phi < 3°$ at 10 sec cadence at 8 GHz are required to achieve this performance.

This requires[4] antenna-based delay noise within 1 ps. In addition to the stochastic contribution, systematic delay drifts will arise from slowly-varying contributions such as the bulk neutral atmosphere (e.g. from differential elevation, particularly when viewing a low elevation target using long baselines) and systematics within the WVRs. The rms noise requirement of 1 ps is used below to derive a requirement for delay drift residual. Before presenting this, a more stringent goal for delay noise is motivated as follows, by considering visibility amplitude loss arising from atmospheric decorrelation in band 6.

The primary approach for minimizing the magnitude of rapid atmospheric delay fluctuations that lead to visibility amplitude loss is to reduce the integration time period (i.e. minimize the integral over the tropospheric temporal structure function). To constrain systematic amplitude loss per baseline ($1 - \exp\left[-\phi^2\right]$; RD07 Equation 7.34) to within 3% at 90 GHz (CAL0403; see Section 5.4.2), antenna-based phase rms errors must satisfy $\phi < 10^\circ$ (or delay noise limit of 300 fs) within an integration period. Using Equation 4 from RD14, this can be achieved by sampling visibilities no slower than every 1.8 sec. To meet the tighter requirement for system electronics of no more than 1% baseline-based amplitude loss (SYS1502), the constraints are $\phi < 6^\circ$ (or delay noise limit of 180 fs) and visibility sampling at 1 sec cadence. For comparison, in the absence of atmospheric decorrelation, an integration time of 0.1 sec is required to keep time smearing loss below -20 dB at the primary beam half-power contour for 18 m dishes over 1000 km baselines of the MA, independent of frequency [RD07 Equation 6.81]. For 6 m antennas over 60 m baselines of the SBA, the maximum integration time is 9 min, again independent of frequency. Therefore, in general, smearing losses will dictate integration periods for the MA, while (frequency-dependent) atmospheric amplitude decorrelation losses will dictate integration periods for the SBA. While WVR data will not be relevant/useful for countering visibility amplitude decorrelation[5], it would be helpful for the WVR's to sample the troposphere with 1 sec cadence. This would supply independent and continuous delay solutions that can be used to monitor conditions and identify any periods when the trend-subtracted variance exceeds the level anticipated to induce 1% baseline amplitude decorrelation at 90 GHz (180 fs). It is also worth noting that, in general, visibility amplitude loss will lead to loss in sensitivity. However, this can be mitigated in cases where it is possible to identify visibilities dominated by sky emission rather than noise. Using CASA terminology, and if WVR data are available on 1 sec cadence, then the WVR trend-subtracted sample-to-sample delay variance can be used to correct for amplitude loss for those visibilities associated with the model (cleaned) data, prior to combination with the residuals.

The timescale over which delay drifts can be corrected is given by the timescale over which standard calibrator referencing will be performed. To satisfy 90% on-target observing efficiency (SYS1061) while seeking to attain 45 dB dynamic range at 8 GHz, and assuming a worst-case 30 sec calibrator referencing

[4]Note that this requirement has been derived assuming that contributions from atmospheric constituents other than water vapor are negligible. While this is likely to be appropriate, further study [RD27, in prep.] is needed to determine the relative contribution toward the 45 dB dynamic range requirement from density and temperature fluctuations in the dry atmosphere.

[5]Unless WVR delay correlations are applied to the pre-correlation data streams per antenna. This approach is not advocated here due to considerable and likely prohibitive complexity overheads, but could be of interest as a possible demonstration upgrade during the post-construction operational phase of the ngVLA.

scan including slew times, this requires a minimum 5 min cycle time. A stochastic contribution of 1 ps on a 10 sec timescale will integrate down to 0.2 ps on a 5 min timescale. To ensure that the quadrature sum of the systematic and time-integrated stochastic parts does not exceed by more than 20% the time-integrated stochastic part alone, the systematic delay must be less than 0.1 ps. To relax this requirement, more frequent calibrator referencing will be required, but this will come at the expense of reduced on-target observing efficiency. The delay measurement error σ_τ resulting from observation of an unresolved source with flux density S and single-baseline single-polarization flux density error σ_{bp} over bandwidth $\Delta\nu$ is given by $\sqrt{3}\sigma_{bp}/(\pi S \Delta\nu \sqrt{N-1})$ [RD07 Equation 9.178]. Assuming 2 GHz RFI-free bandwidth in band 2 (setting this conservatively within the 3.5 GHz IF bandwidth) and taking expected $\sigma_{bp} = 1.5$ mJy/b in 20 sec (approximate maximum allowed without including slew time to meet 90% on-target observing efficiency), a calibrator with minimum flux density 0.5 Jy is required to measure delays to within 0.1 ps. This should be achievable (though may require setting a maximum baseline length for obtaining calibration solutions to ensure sufficient sky density of calibrators with sufficient surface brightness, or ideally unresolved flux density, on the longest baselines approaching 1000 km).

The equivalent derivation to satisfy 35 dB at 27 GHz using $N = 19$ antennas in the SBA yields a requirement for antenna-based phase error of $\phi < 10^\circ$ to be tracked with 8 sec cadence over a 7 hour observation on-target (constrained to be double the 18 m observation time used above; see RD44). Fast switching is not an optimal (nor likely feasible) solution to meet this requirement, where high on-target observing efficiency is sought (SYS1061). Self-calibration is also not ideal (nor likely feasible). Self-calibration requires a compact source with a minimum flux density of 35 mJy (calculated following equivalent approach described for the 18 m main array in RD14, and assuming that the sensitivity of the 6 m array simply scales from the 18 m sensitivities by the number of antennas and the dish diameters [RD45]). While such sources should be plentiful, they are also likely to be contaminated by the target's complex emission at the angular scales of relevance for the short baseline array, rendering them sub-optimal for self-calibration. This also poses risk to any paired-array calibration approaches. Therefore, as similarly deduced for the 18 m antennas, radiometry is the only practical calibration strategy capable of supporting the 35 dB requirement with the 6 m antennas. The longest baseline in the short baseline array is anticipated to be 60 m (i.e. < 80 m). It is therefore conceivable that WVRs could be completely avoided in the 6 m array, instead utilizing a nearby WVR (or array of nearby WVRs) from an 18 m antenna located within 80 m. However, this approach is disfavored as it would likely introduce complexity and conflicts in the future when, for reasons of observational efficiency, different science projects are scheduled on the 6 m and 18 m arrays. Instead, the 6 m array requires its own radiometric capability. While this could be satisfied in principle with only a single WVR-equipped antenna, the need for operational redundancy (given the reasoning above) requires that at least two 6 m antennas are fitted with WVRs.

For the 6 m antennas, using Equation 6 from RD14 with $N = 19$ and 8 sec calibration timescale over 7 hours on-target ($M = 3150$), the image dynamic range limit as a function of frequency ν in GHz arising from tropospheric phase fluctuations, independent of weather conditions (short of observing through thunderstorms), is predicted to be

$$D_{tropo,SBA} \approx \frac{10^{4.9}}{\nu} \quad . \tag{7}$$

Antenna-based phase errors $\phi < 10^\circ$ at 8 sec cadence at 27 GHz are required to achieve this performance. This requires antenna-based delay noise within 1 ps. The stochastic contribution on an 8 sec timescale will integrate down to 0.2 ps on a 5 min timescale. As above, the systematic delay drift must therefore be less than 0.1 ps. Following the delay measurement error calculation above, but now assuming at least 6 GHz RFI-free bandwidth in band 4 (i.e combining data from at least 2 IF bands, but still within the maximum available 13.5 GHz RF bandwidth), and taking expected $\sigma_{bp} = 9$ mJy/b in 20 sec with 6 m antennas, a calibrator with minimum flux density 2 Jy is required to measure delays to within 0.1 ps. This is unlikely to be generally feasible. If instead a minimum flux density of 0.7 Jy is adopted, then a calibrator observation time of 3 min is required. This yields only 40% on-target observing efficiency when enveloped within the necessary 5 min cycle time dictated by the delay drift requirement. While not ideal, this is allowable because 90% efficiency in SYS1061 is a goal rather than a requirement. Future work is required to assess alternate approaches (e.g. self-calibration) or to potentially revise the image dynamic range requirement for the SBA. For now, to avoid complexity with slightly differing delay requirements on the 6 m and 18 m arrays, a requirement of 1 ps rms delay noise in 8 sec will be adopted for all 6 m and 18 m antennas, with 0.1 ps delay drift over 5 mins. Similarly, a common goal of 180 fs delay noise in 1 sec is adopted.

The ability to connect delays over antenna slews is required (e.g. RD16). Delay differences between a calibrator and target field could be as large as 1 ps (temporal structure function) after slewing for 7 sec (CAL0207) to traverse 3° on the sky, or ~ 80 m horizontal difference between tropospheric pierce points at assumed 1500 m tropospheric elevation, with assumed zero advection. Tropospheric advection over baselines to each antenna of interest will contribute additional delay. If not accounted for, the delay difference will alias into the delays measured per calibrator referencing timescale (5 min). As 1 ps exceeds the instrumental drift requirement of 0.1 ps derived earlier, this additional atmospheric error will effectively inhibit the ability to satisfy the image dynamic range requirements (SYS6103) unless it is tracked between calibrator and target. This is captured in CAL0303. Note that if WVR is selected for the IADCS, CAL0303 will require absolute radiometry and in turn careful control over factors like elevation gain dependence and temperature stabilization.

Differences in the positional reference frames between observations in a multi-epoch dataset (with indefinite elapsed time between epochs) could limit high dynamic range imaging when the data are combined in the visibility domain. To attain 45 dB image dynamic range at 8 GHz (SYS6103), phase errors must be minimized [RD03]. The maximum acceptable systematic phase offsets between multiple observations can be estimated as follows. To satisfy SYS6103, Equation 5 indicates that systematic antenna-based phase errors per observation must be smaller than 0.1°, assuming $N = 107$ antennas, 2 observations of 2 hours each (totaling 3.5 hours on target with 90% observing efficiency), and where 2 hours is selected as a modest scheduling block length accounting for weather and declination. The phase measurement error σ_ϕ resulting from observation of an unresolved source with flux density S and flux density measurement error σ is given by $\sigma_\phi = \sigma/S$ [RD07 Equation 9.67]. The anticipated full-bandwith continuum sensitivity in just 1 min at 8 GHz using $N = 107$ antennas will be sufficient to deliver 0.001% flux density uncertainty (50 dB dynamic range) on a 0.4 Jy unresolved calibrator, yielding $0.006°$ per antenna. Therefore, there should always be sufficient signal to noise on the complex gain calibrator to obtain suitable phase self-calibration solutions per observation and in turn align the positional reference frames between observations. An equivalent calculation for the SBA to align two observations totaling 7 hours on target also indicates sufficient signal to noise, where integrating for at least 30 min at 27 GHz yields 0.009% flux density uncertainty (40 dB dynamic range) on a 0.4 Jy unresolved calibrator. While this strategy invokes self-calibration (cf. Section 5.1), this is only required to accurately align multiple observations, rather than being necessary within any given observation. Section 5.4.2 presents a similar calculation but with a focus on amplitude calibration. CAL0305 requires the observatory to deliver scheduling and pipeline capabilities to ensure, where necessary for high dynamic range projects, alignment of flux density scales (and positional reference frames) across multi-epoch observations.

For a 22 GHz WVR to sense the same 18 m atmospheric patch at an assumed height of 1500 m as viewed by an 18 m dish, it will need to be supported by a 1 m dish. A 6 m dish will sense a 6 m atmospheric patch and therefore require a 3 m WVR dish. However, if tropospheric delay corrections are only required every 8 sec (with a goal of 1 sec cadence), and if the tropospheric advection speed is ~ 10 m/s, then a tropospheric patch of 80 m (or as little as 10 m) can be tolerated without degrading capabilities. This in turn reduces the required size of the WVR dish from 3 m to a common size of 1 m for both the 18 m and 6 m main dishes.

If tropospheric delay corrections are only required every 8 sec, and if the tropospheric advection speed is ~ 10 m/s, there will only be a single statistically independent tropospheric delay patch over each 18 m and 6 m dish, respectively. Therefore, direction-dependent (wide-field) corrections for the troposphere will not be required. This is also approximately true (and true within the formal delay noise requirement) when considering the goal of 1 sec cadence for delay corrections.

Similarly, anomalous refraction is unlikely to be of concern. Anomalous refraction describes the wandering of source positions on timescales of seconds, due to refractive wedges of the troposphere with size equal to the antenna diameter moving across the antenna aperture. Anomalous refraction effectively contributes to the pointing error budget (as well as atmospheric delay errors, which are accounted for above). The rms value of the differential phase shift from a wedge is given by the root phase structure function $\sqrt{D_\phi(d)}$ (units of radians) evaluated at a distance given by the antenna diameter d_a. In the case of 3D turbulence (suitable here for ngVLA antenna diameter length scales, e.g. see RD14), the rms value of the anomalous refraction ξ at zenith angle z is given by [RD07 Equation 13.111, corrected without factor $\sqrt{2}$ because $\sqrt{D_\phi(d)}$ is already direction-independent]

$$\xi \approx \frac{\lambda\,(2\pi)^{-1}\sqrt{D_\phi(d_a)\,\sec z}}{d_a}\ \text{rad}\ , \tag{8}$$

where λ is the observing wavelength needed to convert $\sqrt{D_\phi(d)}$ to path length delay in units of distance. When combined with $\sqrt{D_\phi(d)}$ given by Equation 3 from RD14 and assuming a typical tropospheric advection speed of 10 m/s [e.g. RD14], this becomes

$$\xi \approx 2.6 \frac{\sqrt{\sec z}}{d_a^{0.2}} \ \text{arcsec} \ . \tag{9}$$

This relationship is independent of observing frequency. Assuming $z = 60^\circ$ the anomalous refraction is approximately 2.6″ for a 6 m dish and 2.1″ for an 18 m dish. The latter value in particular is approximately the same as the 3″ precision offset pointing requirement (CAL0201). However, given that the timescale < 2 sec for anomalous refraction over dish diameters < 20 m will deliver factor $M > 1$ in Equation 5 compared to the worst-case $M = 1$ calculations assumed for pointing errors presented in Section 5.2.1, anomalous refraction is unlikely to affect the ability to satisfy the 45 dB image dynamic range requirement. Therefore, anomalous refraction will not be considered further here.

5.3.1.2 Ionosphere

The ionized portion of the Earth's atmosphere consists of the ionosphere from about 60–1000 km and the plasmasphere which extends to the plasmapause at approximately geosynchronous altitude. The electron column density is dominated by the ionosphere, which can be approximated by a thin shell at a weighted altitude of ~ 400 km. The ionosphere exhibits structure on all scales ranging from centimeters to the fractional-Earth-circumference bulge caused by the Sun's radiation, with corresponding fluctuation timescales from sub-seconds to hours, and three dimensional drift velocities from m/s to km/s. The ionosphere exhibits strong seasonal and regional dynamics due to the solar cycle, solar inclination, day-night cycle, ionospheric anomalies arising from perturbations such as lightning and tropospheric waves, and the dynamics of ionospheric structures like plasma bubbles, gradients, and traveling ionospheric disturbances. Like the troposphere, ionospheric disturbances can be viewed as a spatial pattern translating across the ground and evolving more slowly in its own reference frame, although unlike the troposphere the diversity of patterns described above makes it difficult to construct generalized predictions for spatiotemporal properties.

The ionized atmosphere will induce an excess delay in units of distance given by [e.g. RD17]

$$\tau_{ion} = -\frac{c^2 r_0}{2\pi\nu^2} \int n_e(l) dl \ \ , \tag{10}$$

where c is the speed of light, r_0 is the classical electron radius, ν is the observing frequency, and the integral over the electron number density n_e yields the total number of electrons per unit area along the line of sight, known as the slant total electron content (STEC). The delay is negative indicating that a monochromatic signal will experience a phase advance relative to vacuum. The corresponding difference in phase between two antennas on a baseline is then given by

$$\Delta\phi_{ion} \approx 480 \, \frac{\Delta N_e}{\nu} \;\; \text{deg} \, , \tag{11}$$

where ν is in units of GHz, and N_e is the STEC in units of 'unit' TEC where $1 \text{ TECU} = 10^{16} \, e^-/m^2$. Assuming uncorrelated lines of sight to each antenna, antenna-based phases will be a factor $\sqrt{2}$ smaller. This assumption is suitable here when focusing on small phase fluctuations on short timescales because GPS observations exhibit a power law of temporal fluctuations extending to sub-second timescales (e.g. RD19; see also the high time resolution VLA observations of ionospheric scintillation presented by RD20). From Section 5.3.1.1, to satisfy SYS6103, antenna-based phase errors must be kept below $3°$ on 10 sec timescales over a 3.5 hour observation $(M = 1260)$ with $N = 107$ antennas to enable 45 dB image dynamic range at 8 GHz. To ensure that ionospheric phase fluctuations do not contribute more than 5% toward the quadrature sum of ionospheric and tropospheric contributions, antenna-based ionospheric phase fluctuations on 10 sec timescales must remain below $\phi < 1°$ at 8 GHz. Using the antenna-based phase-STEC relationship, this requires that STEC can be tracked within 0.02 TECU, or that fluctuations in observed STEC values will remain below this value after removal of a drift slope (sampled on the calibrator referencing timescale 5 min). This translates to antenna-based delay noise $20/\nu^2$ ps where ν is in units of GHz. For SYS6103 specified at 8 GHz, the requirement for antenna-based delay noise arising from the ionosphere is therefore 0.3 ps on 10 sec timescales. Slower variations in the ionospheric electron content must also be removed. As with the troposphere, the timescale over which delay drifts can be corrected is given by the timescale over which standard calibrator referencing will be performed, taken again to be minimum 5 min to satisfy SYS1061. The stochastic contribution on a 10 sec timescale will integrate down to 60 fs on a 5 min timescale. To ensure that the quadrature sum of the systematic and time-integrated stochastic parts does not exceed by more than 10% the time-integrated stochastic part alone, the systematic delay must be less than 30 fs at 8 GHz, or $2/\nu^2$ ps where ν is in units of GHz. To relax this requirement, more frequent calibrator referencing will be required, but this will come at the expense of reduced on-target observing efficiency.

The dynamic range limit as a function of frequency ν in GHz arising from ionospheric phase fluctuations can be predicted by combining the above limit for ionospheric phase fluctuations ($\phi < 1°$ at 8 GHz) with Equation 5, assuming that this limit on 10 sec cadence is satisfied independent of baseline length, antenna location, and ionospheric conditions (assessed below), and assuming $M = 1260$ and $N = 107$, giving

$$D_{ion,MA} \approx 10^{4.1} \, \nu \;\; . \tag{12}$$

Combining Equations 6 and 12, assuming that phase errors from the troposphere $(0.4° \, \nu)$ and ionosphere $(8°/\nu)$ add in quadrature, the dynamic range limit between 1.2–116 GHz arising from atmospheric phase fluctuations is predicted to be

$$D_{atmos,MA} \approx \frac{10^{5.4} \, \nu}{\sqrt{400 + \nu^4}} \;\; . \tag{13}$$

This relationship is displayed in Figure 2. The dynamic range peaks at 46 dB at 4.5 GHz, passes through

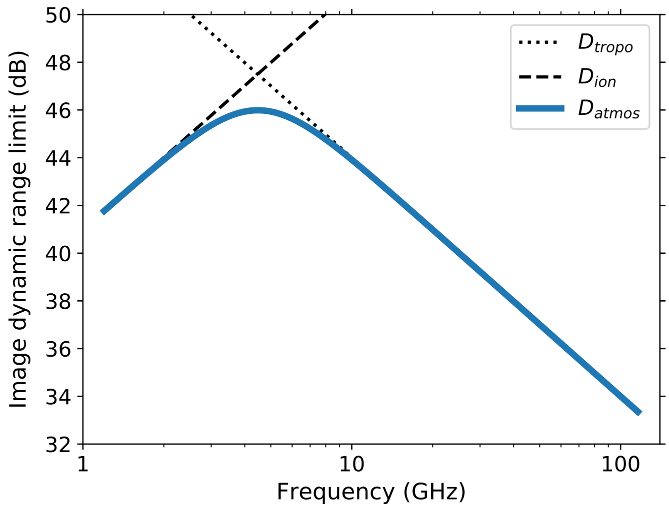

Figure 2 Predicted worst-case image dynamic range limits arising from delay fluctuations in the troposphere (Equation 6), ionosphere (Equation 12), and combined (Equation 13) after a 3.5 hour observation with 107×18 m antennas. All other error contributions (assuming $3''$ precision offset pointing) are negligible by design.

45 dB at 8 GHz and 40 dB at 27 GHz, and drops to 42 dB at 1.2 GHz and 33 dB at 116 GHz. Note that these are worst-case values; the derivations leading to Equation 13 incorporate several worst-case assumptions (e.g. ionospheric delays fluctuate at their predicted upper limits, no self-calibration).

For the short baseline array with $N = 19$ antennas, accepting the above limit for ionospheric phase fluctuations ($\phi < 1^\circ$ at 8 GHz, but assuming that it refers to 8 sec cadence rather than 10 sec; negligible $\sqrt{10/8} = 1.1$), and assuming a 7 hour observation ($M = 3150$) to be consistent with the tropospheric dynamic range prediction from Equation 7, the dynamic range limit arising from ionospheric phase fluctuations is predicted to be

$$D_{ion,SBA} \approx 10^{3.6}\,\nu \quad . \tag{14}$$

Combining Equations 7 and 14, assuming that phase errors from the troposphere $(0.4^\circ\,\nu)$ and ionosphere $(8^\circ/\nu)$ add in quadrature, the image dynamic range limit arising from atmospheric phase fluctuations is predicted to be

$$D_{atmos,SBA} \approx \frac{10^{4.9}\,\nu}{\sqrt{400 + \nu^4}} \quad . \tag{15}$$

This relationship is displayed in Figure 3. The dynamic range is 37 dB at 1.2 GHz, peaks at 41 dB at 4.5 GHz, passes through 35 dB at 27 GHz (satisfying the relevant image dynamic range requirement for the SBA), and drops to 28 dB at 116 GHz. As earlier, these are worst-case values.

To assess whether the 0.3 ps delay noise requirement at 8 GHz is realistic or not, the following preliminary material is presented from RD18 (in prep.) which focuses on statistics of the ionosphere and implications

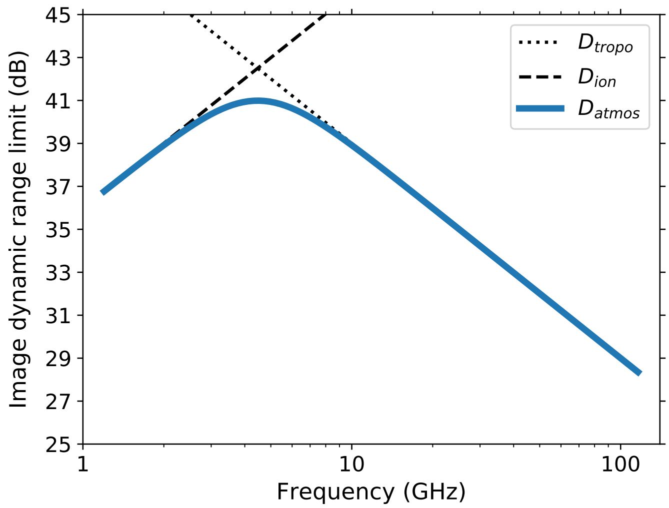

Figure 3 Predicted worst-case image dynamic range limits arising from delay fluctuations in the troposphere (Equation 7), ionosphere (Equation 14), and combined (Equation 15) after a 7 hour observation with 19×6 m antennas. All other error contributions (assuming $8''$ precision offset pointing) are negligible by design.

for phase calibration (i.e. the ionospheric equivalent of RD14). The following data provide a useful and robust reference point, but require further evaluation and comparison with other data before the conclusions should be fully accepted. VLA observations of the calibrator 3C84 presented by RD20 were obtained. The data selected for analysis were observed on 2 Jan 2015 at 00:10 UTC (5:10 pm local time) in C configuration (maximum 3 km baselines) at 1.4 GHz over 100 MHz bandwidth in a single polarization for duration 2 min with 1 sec time sampling. These data exhibit ionospheric scintillation (see RD20). This epoch is near the peak of solar cycle 24, and at a time when the solar elongation was $133°$. The X-ray Sensor on board the *GOES*-15 satellite indicates that all solar flares in the 5 days preceding the observation were of mid-range C class or lower. Reconstructed vertical total electron content (VTEC) data from the International Global Navigation Satellite System Service (IGS), interpolated spatially at the VLA site from GPS data sampled every 2 hr on a grid $2.5° \times 5°$ (lat. × long.), indicate a rapid drop in electron content with rate 8 TECU/hr over a period of 2 hr centered on 00:00 UTC (typical of conditions at sunset). STEC values, interpolated from the VTEC maps, are around 23 TECU with line-of-sight differences between antennas of no more than 0.03 TECU. The phase time series for each baseline was recovered following RD14, yielding temporal structure functions (growth of rms phase fluctuations on a baseline over time) binned by baseline lengths in the ranges < 0.2 km, 0.2–2 km, and 2–3 km. The brief 2 min duration of the input data implies that statistics are degraded at time lags greater than a few seconds. However, this should be just sufficient here where the focus is on 10 sec timescales. The data indicate baseline-based phase fluctuations $< 1°$ on 10 sec timescales at 1.4 GHz, independent of baseline length. Using Equation 11 this equates to STEC fluctuations < 0.003 TECU.

This value is a tenth of the requirement presented earlier. However, it is not yet clear whether the magnitude of fluctuations revealed above are typical or atypical. Similarly, the present data do not answer whether 0.02 TECU fluctuations at 10 second cadence are rare or not. This requires an investigation into the scaling (or lack thereof) with overall STEC values, and with baseline length (e.g. over continental scales), for a range of representative observing conditions. The observations above took place during a time of rapid recombination of the ionosphere, under reasonably active solar conditions (though without significant flaring or coronal mass ejection contributions), so it is reasonable to assume that the ionosphere was in a more excited state than usual. However, there are examples of ionospheric disturbances that become enhanced under quiet solar conditions (solar minimum) such as equatorial spread F (a Rayleigh-Taylor like instability prevalent near the magnetic equator in which the underside of the F region becomes highly turbulent during the post-sunset period, and which is suppressed by solar activity; similar phenomena may exist at the $\sim 40^\circ$ magnetic latitude of the VLA site).

Thus, the tentative conclusion is that ionospheric phase fluctuations will not be an impediment to satisfying SYS6103. Furthermore, these fluctuations will not need to be explicitly tracked on fast 10 sec timescales. However, changes in the ionosphere on the delay drift timescale (5 min) will need to be tracked. GPS-derived VTEC maps from the IGS or other similar services have best-case accuracies $\sim 1\%$. These will not be sufficient to achieve 30 fs drift accuracy at 8 GHz (these are, however, sufficient to correct for ionospheric Faraday rotation which is sensitive to the STEC above each antenna rather than the much smaller difference in STECs between antennas on a baseline; see Section 5.6.3). Instead, the ionospheric delay $\propto \nu^{-2}$ will need to be measured from the observational data (i.e. by fitting the phase change $\propto \nu^{-1}$ in the parallel hand visibility data over an observing band; see e.g. RD21). This leads to several demands on design.

First, the optimal band for performing such measurements is band 1 where ionospheric delay fluctuations will be largest. $2/\nu^2$ ps implies a phase difference of 0.4° over the frequency range 1.2–3.5 GHz. Taking into account the anticipated sensitivity of the ngVLA in band 1 with $N = 107$ antennas, and using the relationship between phase measurement error σ_ϕ resulting from observation of an unresolved source with flux density S and flux density measurement error σ given by $\sigma_\phi = \sigma/S$ [RD07 Equation 9.67], the flux density necessary to measure antenna-based $\sigma_\phi = 0.1^\circ$ within a 200 MHz RFI-free dual-polarization bandwidth in 2 sec is 0.5 Jy. This is realistic for a nearby phase calibrator in band 1. Note that this flux density is an upper limit because the true delay fit uncertainty may be better estimated using the full band 1 bandwidth (an order magnitude larger than 200 MHz). This leads to two options when considering how to implement this in band 2 (or higher frequency bands if ionospheric conditions are particularly poor): the feed could be designed to switch rapidly between bands, or the feed could be designed to support simultaneous observations. The former option would prevent tracking of fluctuations on timescales faster than 5 min (unless SYS1061 can be relaxed), though this could be offset by suitable monitoring of ionospheric conditions as described below. The latter option is not available in the current ngVLA design, though it is not strictly ruled out in the future (in the current design, when not on-axis, the band 1 feed points to open sky; modifications to facilitate some forward gain are likely to incur significant complexity and cost penalties). If it were available, the band 1 feed would be out of focus during band 2 on-axis observations, but the wide field of view from 18 m dishes could in principle enable ionospheric phase fluctuations to be tracked on timescales shorter than 5 mins and perhaps tens of seconds (depending on signal to noise over that interval). This would enable the ionosphere to be tracked in a similar way to that of the troposphere using radiometry. CAL0206 focuses on the former option and requires the ability to perform regular and rapid band switching (which will have implications for maintenance). The switching timescale is required to be no worse than that from CAL0207 (7 sec including settling time). CAL0306 requires a fully automated pipeline data analysis capability to measure and correct for ionospheric delay fluctuations using observations of a calibrator at the phase center, with the goal to expand this capability to arbitrary fields (where requirements on those fields are yet to be defined; the wide field of view of an 18 m dish combined with the high sky density of bright sources in band 1 should ensure that a sufficiently strong celestial signal should always be available regardless of pointing vector).

Second, the ratio of only ~ 10 between the maximum allowable STEC fluctuations (0.02 TECU) and the observed STEC fluctuations (0.003 TECU) indicates that, for contingency, regular monitoring of regional ionospheric conditions must be facilitated for scheduling. CAL0307 requires real-time spatio-temporal GPS-derived monitoring data to be utilized when scheduling observations on the ngVLA, for example using an index like the ROTI (rate of TEC index; e.g. available from the Ionosphere Monitoring and Prediction Center[6]) or the DIXSG (disturbance ionosphere index spatial gradient; RD22). Another useful tracer is the planetary K index.

And third, to ensure optimal scheduling, CAL0308 requires the proposal process to capture the estimated image dynamic range limit, so that degraded ionospheric conditions may be utilized where appropriate. Similarly, CAL0309 requires the scheduler to be capable of starting and stopping scheduling blocks depending on weather conditions across the array, and to account for previously stopped observations in the queue ranking process. Note that it is not clear that adding GPS receivers to ngVLA antennas will be of sufficient benefit, unless they can be programmed to accurately track phase fluctuations by selecting GPS satellites close to the real-time antenna pointing vector. In this case, GPS units could be utilized in an equivalent manner to WVRs and incorporated into the independent delay calibration subsystem. This approach is not yet strictly ruled out, but it is not promoted here because of the larger complexity, risk, and cost compared to measurement of ionospheric phases from the observational data.

The ~ 400 km height of the ionosphere implies that the electron column density will differ for different lines of sight toward the same antenna (the half-power half-beam-width for an 18 m dish at 8 GHz is 3.6′, which corresponds to a lateral distance ~ 400 m at the height of the thin-shell ionosphere). If it is accepted from the results presented earlier that the ionosphere is not dominant at 8 GHz, then SYS6103 does not strictly demand the availability of direction-dependent corrections to account for wide-field distortions from the ionosphere. However, as argued above, it remains plausible (pending further investigation) that the ionosphere could exhibit larger fluctuations that would reduce the dynamic range limit below 45 dB at 8 GHz. These time periods could (perhaps) be sufficiently frequent that they

[6] https://impc.dlr.de/

would be difficult to avoid through scheduling choices. A requirement to implement direction-dependent calibration capabilities in the workflow is not currently recommended, though this requires further study before a final decision should be made. Direction-dependent calibration capabilities would certainly be useful in band 1.

5.3.1.3 Interplanetary Medium

While not part of the Earth's atmosphere, the ionized interplanetary medium is turbulent and will induce phase fluctuations over the array. This may be of scientific interest to some observers and problematic for others. CAL0310 requires that estimates of the minimum acceptable angular offset from the Sun shall be calculated (e.g. RD23) from real-time data sources and fed into the scheduler for optimal array management. This will also need to account for real-time transient alerts for events like solar flares and coronal mass ejections (e.g. using the CACTus quicklook catalog[7] from the LASCO instrument on board the *Solar and Heliospheric Observatory* satellite).

5.3.2 Source Location

Parameter	Req. #	Value	Traceability
Geometric Delay Calibration Residual	CAL0301	Residuals shall satisfy 0.1 ps drift over 5 min for motions over 3° on the sky, 30 fs noise rms on delay tracking timescale	SYS6102, SYS6103, CAL0207, CAL0303
Delay Model Accountability	CAL0315	Real-time applied delays shall be stored so they can be un-applied if needed during post-processing.	CAL0301
Coordinate Equinox	CAL0302	System shall adopt J2000.0 but with flexibility to change in future	–

SYS6102 requires relative astrometric accuracy $< 1\%$ of the synthesized beam FWHM for a bright $(\mathrm{SNR} > 100)$ point source. The astrometric accuracy of an observation results from a combination of statistical errors (uncertainty in calibrator positions, centroid measurement) and systematic errors (reference frame positioning). Uncertainty in calibrator position will not be considered here, though the calculation is similar to that presented below accounting for both first and second order errors [see RD07 Sec. 12.2.3 and A12.2, also RD08 Sec. 5.4]. The centroid error within a reference frame is given by $\mathrm{FWHM}/(2\,\mathrm{SNR})$, which is $< 0.5\%$ of the beam for $\mathrm{SNR} > 100$. To ensure that the combination of all

[7] `http://sidc.oma.be/cactus/`

position errors remains below the 1% requirement, the reference frame must be accurately positioned, in turn requiring accurate calculation of the geometric delay τ_g (among other delays).

For absolute astrometry, the precision of the applied geometric delays (i.e. delay model accountability, or knowledge of the precise delays that were applied as a function of time) is of greater importance than their accuracy because the latter can be corrected (within reason, as examined below) in post-processing as part of the delay model fitting procedure. For maximum baselines $B = 9000$ km at 116 GHz, the synthesized beam FWHM is 60 μas. To point the delay tracking center to within 0.5% of a beam ($\Delta\theta = 0.3$ μas), it is required that the applied geometric delay is known to within $\Delta\tau_g < B\Delta\theta/c = 40$ fs. This requirement will ensure that geometric delays do not limit the absolute astrometry down to 1% of the FWHM. This calculation effectively assumes $M = 1$ statistically independent snapshots; this is appropriate here. The corresponding antenna-based delay precision is 30 fs.

The relative astrometric accuracy can be estimated by considering gain calibration, where the delay toward a target source will be corrected using the delay toward an adjacent calibrator located at separation angle $\theta_{\rm sep}$. The relative astrometric uncertainty will be dictated by any delays that differ at the two locations, in this case focusing on inaccurate geometric delay tracking. The relative positional uncertainty is calculated using the equation for absolute positional uncertainty, but improved by the factor $\theta_{\rm sep}$ [RD07 Sec. 12.2.3, RD08 Sec. 4.1]. Thus, assuming a worst-case 3° separation (following CAL0207), the required accuracy for geometric delay is given by $\Delta\tau_g < B\Delta\theta/(c\,\theta_{\rm sep}) = 0.8$ ps over a (minimum) 5 min calibrator referencing timescale. The corresponding antenna-based delay accuracy is 0.6 ps. This is the accuracy needed for correlation. However, this is insufficient to ensure that systematic errors will be dominated by the troposphere for imaging dynamic range requirement SYS6103. To ensure that this is satisfied, antenna-based delays must be within the tropospheric drift constraint of 0.1 ps over 5 min from CAL0303.

Both the 0.1 ps accuracy and 30 fs precision requirements are needed in order to satisfy the most flexible reading of SYS6102; absolute astrometry is effectively relative to a global reference frame.

The 0.1 ps requirement sets a limit for combined delay drifts from antenna location, antenna structure, and electronics. Dividing this requirement by factor $\sqrt{3}$, these components, discussed below in Sections 5.3.3, 5.3.4, and 5.3.5 respectively, are each assigned a drift allocation of 60 fs.

The ngVLA should plan to use J2000.0 coordinates, including full corrections for time and motion of the Earth and solar and planetary gravitational deflection [RD07 Sec. 12]. However, it is possible that an IAU adopted frame replacing J2000.0 may become available during the lifetime of the ngVLA (perhaps even as a result of ngVLA measurements). For example, the clear detection of galactic acceleration (secular aberration[8]) in the existing J2000.0 frame (> 150 μas over 30 years) has motivated the proposal for an epoch ICRF [RD10]. Thus, flexibility should be provided; nowhere in the project should J2000.0 be assumed.

[8] Peculiar acceleration arising from the motion of the Sun with respect to the local standard of rest is expected to be an order of magnitude smaller than galactocentric acceleration [RD09].

For radio sources located within approximately 30 light years, the near-field effect of the curvature of the wave front will need to be accommodated in the delay model (e.g. see Section III.A.2 from RD17).

Future work is required to determine if corrections are needed for differential aberration between antennas [RD43]. This effect introduces an additional phase term in the measurement equation similar to that arising from non-coplanar w-terms. Image dynamic range limitations resulting from this effect on long baselines (1000's of km) may be acceptable without compensation.

5.3.3 Antenna Location

Parameter	Req. #	Value	Traceability
Antenna Pad Location Calibration Residual	CAL0311	Residuals shall satisfy 0.5 mm 3D radial error, or equivalently 0.3 mm 1D rms error for each of 3 dimensions, after removing systematic drifts for 18 m antennas. For 6 m antennas the requirements are 0.2 mm (3D) and 0.1 mm (1D).	SYS1501, SYS6103, CAL0207, CAL0301
Timing Accuracy Across Baselines	CAL0312	Timestamp accuracy shall be within 10 μs rms over 1000 km baselines with 18 m antennas. The requirement for 6 m antennas is 70 ms rms over 60 m baselines.	CAL0311

The relative positions of the antennas must be accurately determined so that geometric delays can be correctly calculated and supplied to the correlator. Residual delays due to incorrect antenna locations will result in differential phase errors between sources separated on the sky (as examined from the perspective of source location in the previous section) and will in turn limit image dynamic range.

To ensure that systematic errors are dominated by the atmosphere and not antenna location errors (SYS1501), the residual systematic delay following a 3.5 hour observation with 5 min calibrator referencing ($M = 42$) to support 45 dB image dynamic range at 8 GHz with 107×18 m antennas (SYS6103) must be within $\tau_{sys,MA} = 0.9$ fs. This is calculated by reducing the antenna-based delay drift requirement of 60 fs (see CAL0301 and allocation described in Section 5.3.2) by factor $\sqrt{NM}$ with $N = 107$. The required baseline accuracy is then obtained by considering the phase error arising from sources separated on the sky [RD07 Sec. 12.2.3], given by $\Delta B < c\tau_{sys,MA}\sqrt{N_b M_b}/\theta_{\rm sep}$ where N_b is the number of baselines and M_b is the number of statistically-independent baseline settings over an observation. The residual errors from N_b baselines are assumed to be statistically independent, justified by the variety of trigonometric factors that contribute to fringe phase and the prior removal of systematic antenna location drifts. Assuming a worst-case 3° separation (following CAL0207), $N = 107$ (i.e. $N_b = 5671$), and worst-case $M_b = 3.5$ (i.e. any residual baseline error is only statistically independent for 1 hour at most; this is appropriate for multi-hour observations relevant for high dynamic range imaging here, throughout which diurnal tides are acting), the required baseline accuracy is then given by 720 μm. The corresponding requirement for maximum error on an individual 18 m antenna location determination is then then 510 μm (this assumes that errors add in quadrature, which not true for any given baseline but is a reasonable assumption when averaged over the array). This is 5 times smaller than the wavelength at the ngVLA's upper frequency bound of 116 GHz.

This is expected to be an accessible level of accuracy to measure using global fringe fits to of order 100 point sources sampling the entire sky [e.g. RD07 Sections 4.5 and A12.1]. Note that the timescale for a complete turn of phase (inverse of residual fringe rate) arising from a baseline error is approximately $c/(\nu\omega_e\Delta B)$, where $\omega_e = 7.3 \times 10^{-5}$ rad/s is the rotation rate of the Earth. To illustrate, this is > 9 hr at 116 GHz for $\Delta B < 1$ mm and even longer at lower frequencies. However, the need to maintain accuracies within 1 mm over time are likely to present a challenge. Techniques from VLBI will be needed in order to model and remove predictable drift from the error budget (e.g. see extensive discussion in RD17), including diurnal motions such as tides (~ 0.5 m), ocean loading, and Earth polar motions, and slower systematic trends from tectonic plate motions. Regular antenna position calibration campaigns will be required (e.g. monthly).

The equivalent derivation to facilitate 35 dB image dynamic range at 27 GHz following a 7 hour observation with 5 min calibrator referencing ($M = 84$) with 19×6 m antennas yields $\tau_{sys,SBA} = 1.5$ fs, baseline accuracy within 300 μm, and antenna location accuracy within 210 μm. While this may appear to be even more challenging than the requirement derived above for 18 m antennas, note that antenna position errors are expected to be highly correlated in their bulk motions over the maxmimum 60 m baselines of the SBA. As a result, it is conceivable that a 210 μm requirement for 6 m antenna location accuracy can be met in practice.

The antenna positional requirements presented above are residual (systematic drifts removed) 3D radial errors, i.e. the mean (Euclidean norm) of a chi distribution with three degrees of freedom, where the mean is factor $\sqrt{8/\pi}$ larger than the equivalent 1D rms error along each of 3 dimensions.

The antenna location accuracy also provides a worst-case requirement for the timing accuracy across the array Δt constrained by $\Delta B \sim \omega_e \Delta t B_{\rm max}$. This is needed to avoid time-consuming searches for fringes (though this calculation should be assessed more carefully in the future to determine how poorly the timing accuracy can be reduced without exceeding reasonable computational resources during fringe searches and without incurring systematic timing errors that exceed those from time-variable antenna location errors). For 720 μm accuracy over 1000 km baselines of the MA (longest baselines relevant to SYS6103) this implies a timekeeping accuracy of $\sim 10\,\mu$s. For 300 μm accuracy over 60 m baselines of the SBA this implies a timekeeping accuracy of ~ 70 ms. Note that these timescales are orders of magnitude faster than anticipated integration times of ~ 0.1 sec for MA and as short as ~ 1 sec for SBA (as derived earlier in Section 5.3.1.1).

5.3.4 Antenna Structure

Parameter	Req. #	Value	Traceability
Antenna Structure Delay Calibration Residual	CAL0313	Residuals for 6 m and 18 m antennas shall satisfy 60 fs drift over 5 min for motions over 3° on the sky, 100 fs noise rms in 1 sec	SYS1501, SYS1502, CAL0207, CAL0301

The antenna structures and their motion will contribute delay (e.g. RD17). These can be thought of as modifications to the antenna location. For example, the Earth's orbital velocity $10^{-4}c$ must be taken into account to achieve mm accuracy. This motion causes Lorentz effects of order $10^{-4}L$, which for a 10 m axis offset is 1 mm or 3 ps.

Repeatable parts of the antenna structure delay include the change of main reflector shape with elevation or azimuth, axis non-intersection, illumination offset, bearing runout, and bearing alignment. Most of this repeatable component can be accurately predicted through careful measurements. Non-repeatable (and typically not predictable) parts of the antenna structure delay include thermal[9] and wind deformation of the main reflector shape and feed position, and bearing non-repeatability. The magnitude of each of these contributions, particular from the non-repeatable factors, will likely only be determined by experimentation over time with the constructed ngVLA antennas.

In order for the delay budget to be dominated by the atmosphere rather than the instrument (SYS1501), the systematic part of the antenna structure delay must be less than 60 fs in 5 min (see CAL0301 and allocation described in Section 5.3.2). Note that the timescale over which systematic antenna structure delays can be corrected is given by the 5 min calibrator referencing timescale justified in Section 5.3.1.1. Following CAL0207, the systematic requirement relates to motions within a 3° solid angle on the sky. Scaling by the square root of the timescale ratio, the systematic requirement translates to a stochastic noise level of 1 ps on 1 sec timescales. However, a more restrictive requirement for the delay noise component is derived by constraining systematic amplitude loss per baseline ($1 - \exp{[-\phi^2]}$; RD07 Equation 7.34) to within 1% (SYS1502). This requires antenna-based phase rms errors $\phi < 6^\circ$ at 116 GHz, or delay noise 140 fs (i.e. SYS1503), on 1 sec timescales. Both the antenna structure and the electronics (examined in the following section) contribute to this total. Therefore, dividing by factor $\sqrt{2}$, the requirement for the antenna structure delay noise residual is 100 fs in 1 sec. The drift and noise requirements are relevant for all 6 m and 18 m antennas. To relax the drift requirement, more frequent calibrator referencing will be required, but this will come at the expense of reduced on-target observing efficiency.

[9] A rough estimate for the expected thermal expansion rate can be obtained by multiplying the dish diameter by the thermal expansion coefficient, which for a steel 18 m dish is approximately 600 fs/$^\circ$C.

5.3.5 Electronics

Parameter	Req. #	Value	Traceability
Electronics Delay Calibration Residual Per Polarization	CAL0314	Residuals per polarization for 6 m and 18 m antennas shall satisfy 80 fs drift over 5 min for motions over 3° on the sky, 70 fs noise rms in 1 sec	SYS1501, SYS1502, CAL0207, CAL0301

There is a component of delay introduced because of the electronics between the feeds on the antennas and the samplers. This will need to be measured for each antenna, receiver, and polarization. The electronics and particularly the local oscillator must be designed so that they are more phase stable than the atmosphere (SYS1501). Following Section 5.3.4, but now dividing by an additional factor of $\sqrt{2}$ to specify the requirement per polarization, the stochastic part must contribute less than 70 fs on 1 sec timescales, and the systematic part must contribute less than 80 fs over a stability timescale of 5 min. These requirements are relevant for all 6 m and 18 m antennas.

5.4 Amplitude

Parameter	Req. #	Value	Traceability
Noise Diode Amplitude Stability	CAL0401	Noise diode amplitudes for 6 m and 18 m antennas shall be stable over the full range of accessible antenna pointing vectors to within 0.3% drift over timescales up to 5 min, 1% drift over timescales up to 1 month	SYS1064, SYS6103, SYS1501, CAL0201
Antenna Elevation Gain Amplitude Dependency	CAL0402	Elevation gain amplitude dependency shall be modeled to within 0.1% at 8 GHz and 1% at 27 GHz per 18 m antenna, and within 0.2% at 27 GHz per 6 m antenna. Goals for other frequencies: best achievable.	SYS6103, CAL0702

Parameter	Req. #	Value	Traceability
Default Amplitude Calibration	CAL0403	Default amplitude calibration shall deliver best-case 1% absolute flux density accuracy added in quadrature with the accuracy at which celestial flux density standards are known at the frequency of interest, for Standard Interferometric Observing Modes using database calibration without overheads, i.e. without needing optimized scheduling (e.g. observing near constant elevation) or specialized calibrations (e.g. offset pointing, antenna dips, observations of celestial flux density standards). Using this approach, goal to deliver no worse than 6% total absolute flux density accuracy.	SYS1061, SYS1064, SYS6101
Calibrator Database: Flux Density Standards	CAL0404	Celestial flux density standards and their flux density ratios shall be monitored every 1 month, with sufficient sources in each frequency band to identify variability in any source.	SYS1063, CAL0405
Internal Absolute Amplitude Scale	CAL0405	Stable internal scaling between cross-product spectral power and spectral flux density on timescales up to 1 month shall be maintained using a switched power system on 6 m and 18 m antennas, utilizing noise diode stability (CAL0401) and elevation-dependent aperture efficiencies (CAL0402) tied to regular monthly observations of celestial absolute flux density standards. This shall include the capability to return an antenna to the array following an inactive period (e.g. due to maintenance).	SYS1063, CAL0403

Parameter	Req. #	Value	Traceability
Switched power RFI mitigation	CAL0406	Signal processing/filtering shall be implemented to prevent RFI from contaminating the switched power system on 6 m and 18 m antennas at levels equivalent to greater than 0.3% in noise diode amplitude stability over timescales up to 5 min.	CAL0401, CAL0405

Two forms of amplitude calibration must be considered. First is the need to deliver accurate relative amplitude calibration, namely stability in the amplitudes measured during an observation. Second is the need to place corrected visibilities onto an accurate absolute flux density scale.

5.4.1 Relative Amplitude Calibration

Relative amplitude calibration is required to ensure amplitude stability within an individual observation in a given instrumental tuning, including in a general sense where that observation could range in elevation from zenith to horizon. To maintain a stable amplitude scale, fluctuations in electronic gain, antenna aperture efficiency, and atmospheric opacity must be considered (e.g. see Equation 1 in RD24). These are addressed in turn below.

Noise diodes placed upfront in the signal path can be used to track changes in electronic gains. The current ngVLA design incorporates one temperature-stabilized noise diode per feed and antenna, with associated bias circuitry to optimize stability in switched power. The noise diodes need to be sufficiently stable to satisfy relative flux scale calibration to 5% precision without the need for tipping scans in standard observing modes (SYS1064), and also to prevent amplitude errors that can limit image dynamic range. The latter is more demanding and drives the following noise diode performance calculation. The image dynamic range limit resulting from antenna-based amplitude errors (correlated for both polarizations on a given antenna) is given by Equation 1. When modified to include the M factor (number of statistically independent samples) from RD03, this is given by

$$D \approx \frac{N\sqrt{M}}{\epsilon} \,. \tag{16}$$

To facilitate 45 dB image dynamic range at 8 GHz (SYS6103) with $N = 107$ MA antennas, adopting a dynamic range target of 48 dB to ensure errors are limited by the atmosphere (SYS1501) and assuming that diode errors are randomized on timescales of ~ 5 min (calibrator referencing timescale) throughout a 3.5 hour observation (following Section 5.3.1.1), antenna-based amplitude errors ϵ must be no larger than 1%. An equivalent calculation to target 39 dB image dynamic range at 27 GHz with $N = 19$

SBA antennas with 5 min randomization timescale over a 7 hour observation yields a requirement for ϵ within 2%. The stricter limit of 1% is selected for all antennas to avoid unnecessary complexity. This is a requirement for timescales up to the length of an observing block (in the following section this requirement will be bounded by a timescale up to 1 month). However, noise diode stability must be better than this on short timescales. To facilitate rapid calibrator modeling (CAL0702), it must be possible to attain 45 dB image dynamic range at 8 GHz for a snapshot observation ($M \approx 1$) with 107×18 m dishes. Using Equation 16, this demands antenna-based on-axis amplitude errors within 0.3%. CAL0401 requires 0.3% amplitude stability over timescales up to 5 min, for both 6 m and 18 m antennas to avoid unnecessary complexity. The noise diode stability requirements above must be maintained over arbitrary changes in antenna pointing vector. The levels of stability demanded above will also satisfy the requirement for 5% relative amplitude calibration from SYS1064.

Gravitationally induced deformation of an antenna's surfaces and support structures will lead to loss in forward gain. This loss is largely predictable as a function of elevation angle. When this elevation gain dependency for an antenna is combined with factors like the illumination taper[10] introduced by the feed, the frequency- and elevation-dependent antenna aperture efficiency can be calculated. As the typically dominant contributor to fluctuations in aperture efficiency, the elevation gain dependency of each antenna must be known accurately in order to minimize amplitude errors and in turn raise image dynamic range limits. Importantly, the combination of accurate elevation-dependent aperture efficiencies and noise diode stability can be used to provide a stable internal absolute flux density scale. The accuracy with which the elevation gain dependency can be predicted from an empirical model is dictated by the pointing error (e.g. see Fig. 2 from RD24). To facilitate 45 dB at 8 GHz with 107×18 m antennas in a worst-case snapshot observation ($M = 1$, to satisfy CAL0702), Equation 16 requires antenna-based amplitude errors within 0.3%. From Equation 2 this can be accomplished on-axis with 14″ pointing. Similarly, to facilitate 35 dB at 27 GHz requires amplitude errors within 3%, which can be accomplished with 13″ pointing. Conservatively, adopting 10″ pointing, the values of ϵ will be 0.2% at 8 GHz and 2% at 27 GHz. It will therefore be possible to model the elevation gain amplitude dependency to accuracies better than these levels for each 18 m dish because this model will be generated by averaging over pointing errors (combined with statistically independent noise diode amplitude errors from earlier). If the systematic contribution is within 50% of the statistical pointing error, given by 0.1% at 8 GHz and 1% at 27 GHz, then their quadrature sum will be inflated by $\sim 10\%$. These accuracies can be constrained at any given elevation using at least 4 independent on-axis measurements (e.g. sampling over a few minutes per elevation). An equivalent derivation for 19×6 m antennas to satisfy 35 dB on-axis dynamic range at 27 GHz with $M = 1$ yields a requirement of 0.2% for antenna-based systematic elevation gain amplitude errors, which can be accomplished with 15″ pointing.

The transparency of the troposphere is affected by water vapor and molecular oxygen. The opacity varies as a function of observing frequency (e.g. see Figure 13.7 from RD07). It also varies as a function of time, primarily as a result of changes in water vapor content, ranging from fluctuations on fast-changing second

[10] If the aperture illumination exhibits significant systematic changes with the antenna pointing vector, then like the elevation gain dependency these will need to be modeled so that aperture efficiency can be accurately predicted.

timescales to slow-changing diurnal timescales. To faciliate 48 dB image dynamic range at 8 GHz (as above), Equation 16 with $N = 107$ MA antennas indicates that antenna-based amplitude errors arising from opacity fluctuations on 5 min timescales over a 3.5 hour observation must be corrected to within 1%. Similarly, to faciliate 39 dB image dynamic range at 27 GHz with $N = 19$ SBA antennas, antenna-based amplitude errors on 5 min timescales over a 7 hour observation must be corrected to within 2%. For comparison, to assess whether these are realistic targets, the limited investigation by RD26 found that opacity at the VLA site at 23 GHz can vary by 0.5% over 30 mins. More detailed statistics of opacity fluctuations are currently being investigated using EVLA switched power data [RD27, in prep.]. The results presented by RD26 suggest the need for a capability to track and correct for changes in opacity on 5 min timescales. Atmospheric brightness temperatures scale exponentially with atmospheric opacity (e.g. Section 13.1.3 in RD07). This relationship is approximately linear for small changes in atmospheric opacity. If the atmosphere dominates the system temperature, then the requirements above can be facilitated by a switched power system underpinned by noise diodes with stability no worse than 1% on 5 min timescales. This is effectively supported by the electronic gain requirement (CAL0401). Note that this argument assumes that visibility errors are dominated by system noise rather than correlated celestial signals. For fields containing strong targets, regular tracking of a nearby blank sky region may be required. Note also that a switched power system is capable of differentiating between changes in electronic gains and atmospheric opacity [RD28].

Ideally, long timescale fluctuations in atmospheric opacity will also need to be tracked by the switched power system (on timescales of an individual observation, or even weeks as described in the next section), such that the use of model opacities or empirical opacities from antenna dips (tipping scans) will not be required. However, this requires future investigation. It may become evident that accuracy under this scheme can only be maintained by calibrating the internal opacity tracking with data from tipping scans. There may also be a need to combine the tipping data with an atmospheric temperature (or better, a vertical temperature profile), because the atmosphere is mostly transparent down to the horizon at frequencies up to 116 GHz and therefore cannot be used to directly infer the atmospheric opacity. If this is required, further investigation will be needed to determine whether atmopsheric models will be sufficient for this purpose, or whether sensing data (e.g. publicly available radiosonde data, or oxygen sounders operating in the wings of the 60 GHz absorption lines) will be required to ensure sufficient accuracy. If it becomes evident that additional calibrations like tipping scans will need to be added to scheduling blocks to facilitate certain scientific objectives (like high dynamic range), then it may be useful (or necessary; see SYS1064) to define a new 'enhanced' amplitude calibration procedure to differentiate from the default procedure in CAL0403. Note that to satisfy SYS6103 at 8 GHz with $N = 107$ MA antennas, the residual systematic antenna-based amplitude error per observation (i.e. $M = 1$) must be within 0.2%. This is also the constraint needed to satisfy SYS6103 at 27 GHz with $N = 19$ MA antennas. While these levels of uncertainty in the amplitude scales between antennas may not be achieved using the internal diode stabilized system (e.g. consider observations performed near the end of the month between celestial re-calibration, when consistency in the amplitude scales maintained between the noise diodes may have degraded), the inclusion within the scheduling block of a celestial flux density calibrator (and other scans like tipping) might not be required because there will likely be sufficient signal to noise on the regularly-observed gain calibrator to align the time-dependent antenna-based amplitude scales. Further work is required to verify these arguments and, if necessary, refine the proposed amplitude calibration procedures and requirements.

Absorption in the ionosphere arises from collisions between electrons with ions and neutral particles and is $\sim 2\%$ at 100 MHz during periods of high ionospheric activity [RD07 Sec. 14.1.4]. This varies with the inverse square of the frequency (i.e. 0.0003% at 8 GHz) and can therefore be neglected here.

5.4.2 Absolute Amplitude Calibration

Uncertainty in the absolute flux density scale assigned to an observation will translate to variability in flux densities measured from the same field at different times, or at different frequencies (unless multiple bands can be observed simultaneously). It is not practical to consider maintaining absolute flux density calibration over an indefinite time period using an instrumental reference source. However, this approach is realistic using noise diodes over approximately monthly timescales, when tied to regular observatory (service mode) observations of celestial flux density standards. If a celestial flux density standard is observed on approximately monthly timescales (at high signal to noise, and employing all necessary optimizations to ensure high accuracy such as observing under precision conditions, minimizing the elevation range over which observations are obtained and avoiding low elevations, and including additional calibrations like regular tipping scans and offset pointing), then the absolute flux density scale can be transferred to the instrumental standard and in turn applied to observations during the month-long time window. Note that at any one time, a number of antennas may be removed from the array for maintenance. To reintegrate these antennas into the array, there will need to be a capability to transfer the internal scale maintained by all active antennas to the returned antennas. This could be achieved using regular (as frequently as daily) brief service-mode observations of bright calibrators with the full array, e.g. in between science blocks. Alternatively, it may be possible to accomplish this using complex gain calibrator data from the science blocks themselves. Heuristics will need to be developed.

SYS6101 is traced to SCI0110 [L0 requirement from AD01] which calls for 1% photometric error. According to the definition in AD01, this is not the fractional error in absolute flux densities, but rather the fractional error in the observed flux densities prior to scaling by a flux density standard. SCI0110 therefore effectively implies that if we measure the flux density for a target source with infinite signal to noise in several independent observations, the absolute amplitude calibration scale maintained internally by the telescope over the time period encompassing all the observations should be sufficiently stable to deliver flux densities within 1% of each other. However, while theoretically possible, it is unrealistic to demand of the ngVLA a stable internal amplitude scale over indefinite time periods. Therefore, periodic referencing of a celestial flux density standard will be inevitably required. As a result, the accuracy in the measured flux densities will be affected by not only the amplitude stability of the instrument, but also the accuracy at which the celestial calibrator's absolute flux density is known (unlikely to be better than 1%, e.g. RD24) as well as any variability that the calibrator might exhibit. To avoid complicating the requirements while satisfying the objective of SCI0110, SYS6101 is interpreted more conservatively in this document in terms of absolute flux density.

To satisfy SYS6101 using the approach above, assuming N statistically independent noise diodes over $N = 107$ MA antennas (i.e. common between polarizations on any receiver), the noise diode amplitudes per antenna must remain stable and not drift beyond 10% of their $t = 0$ values over a 1 month period (i.e. stable to 1% when averaged over all antennas). For $N = 19$ SBA antennas the equivalent drift requirement is 4%. To compensate for any possible systematics between diodes at the few percent level on long timescales (not expected, but not impossible) and to avoid unncessary complexity, the requirement is 1% per-antenna for all antennas. This approach has an additional benefit: uncertainty in the flux density scale between observations performed within the 1 month period between celestial recalibration will be 1% or better (whether the noise diodes are statistically independent or if they exhibit some smaller deviation about a systematic 1% error), independent of the intrinsic accuracy to which the flux density of the celestial standard is known. This feature will likely be of particular interest to those in the community that seek to observe transient phenomena over timespans up to a few weeks (e.g. rising or decaying target brightness). Note that intrinsic accuracy in the flux density scale is currently at best 1%–3% depending on frequency between 1–50 GHz [e.g. RD24], rising to near 5% at 116 GHz [e.g. RD25]. The intrinsic accuracy is approximately 1% at 8 GHz and 2% at 27 GHz.

To improve observing efficiency (SYS1061), CAL0403 defines a default amplitude calibration procedure that minimizes overheads. To illustrate the wording of CAL0403, the absolute photometric accuracy for any individual observation will be given by the quadrature sum of (say) worst-case 1% instrumental stability and (say) 3% uncertainty for a celestial flux density standard at the frequency of interest, yielding 3.2%. This uncertainty (or the worst-case 6% goal defined in CAL0403) also reflects the typical variation expected between flux densities measured from observations taken more than 1 month apart (assuming celestial recalibration takes place on this timescale), though note that uncertainty in the flux density of a celestial standard may be somewhat time-stable (i.e. systematic, yielding improved coherence between observations, with relevance to the transient comment earlier). The 6% goal in CAL0403 accommodates a worst-case 3% residual from atmospheric decorrelation at 116 GHz (see discussion related to CAL0303 in Section 5.3.1.1).

To satisfy CAL0403 using the combination of an instrumentally-maintained absolute flux density scale tied down by regular observations of celestial standards, absolute flux densities for celestial standards at all frequencies of interest (1–116 GHz) must be known to better than 5% (currently satisfied, as above), celestial standards must be monitored every month, there must be a capability to identify and handle (unexpected) variability in celestial standards, and (as would be expected to maintain high accuracy) observations of celestial standards must employ all necessary optimizations and additional calibrations as highlighted above.

To achieve this, a grid containing a reasonably small number of stable (including slowly varying) flux density calibrators situated across the sky will need to be identified and monitored regularly, with flux densities stored in a calibration database (e.g. RD29). There will need to be at minimum a few standard sources available in each frequency band. Observations of all flux density standards should be performed as close together in time as possible (e.g. within 24 hours). Should any of the 'standards' exhibit unexpected variability, this will need to be detected by comparing light curves for flux density ratios between sources. The light curve data should be used to inform decisions about whether to base the internal flux density scale on a (possibly temporarily) reduced subset of 'standard' sources. A timescale of 1 month is required between reobserving the celestial standards so as to minimize impacts on science observing efficiency (note that 90% efficiency implies an allowance of 10% of real-time, i.e. 2.4 hours/day or 3 days/month, for calibrations and array maintenance) while ensuring that variability in flux density standards can be detected (and interpolated where necessary) with sufficient time resolution.

Accounting for all uncertainties, including noise diode stability (CAL0401) used to track fluctuations in electronic gain and opacity, and the predictive accuracy of elevation gain dependencies (CAL0402) used to calculate accurate antenna aperture efficiencies, the absolute flux density uncertainty without the final contribution from intrinsic uncertainty in the celestial scale (between 1%–5%, see earlier) is anticipated to be less than 1% in all frequency bands, irrespective of observing conditions (even for $25''$ blind pointing with 107×18 m antennas in normal conditions at 116 GHz, for example considering a 5 min pointing randomization timescale over a 3.5 hour observation, or for $85''$ blind pointing with 19×6 m antennas with 5 min randomization timescale over a 7 hour observation). When combined with up to 5% uncertainty from the celestial flux density scale at 116 GHz, the total absolute flux density uncertainty could be as large as 6%.

Future detailed analyses are required to validate the anticipated 1% best-case and 6% worst-case absolute flux density uncertainties targeted above, and to decide if the default amplitude calibration scheme will be sufficient in all cases. If not, an 'enhanced' scheme may be required.

Finally, it is important to note that differences in the absolute amplitude scale between observations in a multi-epoch dataset could, when the data are combined in the visibility domain, limit high dynamic range imaging. To facilitate high dynamic range imaging (SYS6103), amplitude errors must be minimized [RD03]. The maximum acceptable systematic offset between amplitude scales in multiple observations can be estimated as follows. To attain 45 dB image dynamic range at 8 GHz with $N = 107$ MA antennas, Equation 16 indicates that systematic antenna-based amplitude errors must be less than 0.5%, assuming 2 observations of 2 hours each (following the similar calculation for systematic phase errors in Section 5.3.1.1). The anticipated full-bandwith continuum sensitivity in just 1 min at 8 GHz using $N = 107$ antennas will be sufficient to deliver 0.0008% flux density uncertainty on a 0.5 Jy unresolved calibrator, yielding 0.008% per antenna. An equivalent calculation to attain 35 dB image dynamic range at 27 GHz with $N = 19$ SBA antennas requires antenna-based amplitude errors to be within 0.8%, assuming two observations totaling 7 hours on target. The anticipated full-bandwith continuum sensitivity in just 1 min at 27 GHz using $N = 19$ antennas will be sufficient to deliver 0.04% flux density uncertainty on a 0.5 Jy unresolved calibrator, yielding 0.2% per antenna. Therefore, there should always be sufficient signal to noise on the complex gain calibrator to obtain suitable amplitude self-calibration solutions per observation and in turn align the flux density scales between observations. While this strategy invokes self-calibration (cf. Section 5.1), this is only required to accurately align multiple observations, rather than being necessary within any given observation. CAL0305, presented earlier in Section 5.3.1.1 with equivalent focus on phase reference frame matching, requires observatory scheduling and data reduction capabilities (pipeline) to ensure, where necessary for high dynamic range projects, coherence in flux density scales across multi-epoch observations.

5.5 Bandpass

Parameter	Req. #	Value	Traceability
Default Bandpass Calibration	CAL0501	Default bandpass calibration shall apply bandpasses from a calibration database with compensation for time-variable opacity, without including bandpass scans in science observation scheduling blocks, nor using calibrators from the data to measure the bandpass.	SYS1063, SYS1066
Instrumental Bandpass Accuracy	CAL0502	The observatory shall measure bandpasses for 18 m antennas with accuracies per polarization of 1% in amplitude and 0.3° in phase within 0.1 km/s channels between 16–50 GHz (goal: all frequency space), taking care to ensure that tropospheric and ionospheric systematics are removed to within these accuracies. To enable more accurate solutions to be obtained over broader channels by averaging the 0.1 km/s solutions, the latter shall be measured and stored in a way that enables accountability of various filter responses (baseband, subband). Bandpass accuracy goals for 6 m antennas are 10% in amplitude and 3° in phase within 0.1 km/s channels across all frequency space.	SYS6105, SYS6106

Parameter	Req. #	Value	Traceability
Instrumental Bandpass Stability	CAL0503	The systematic instrumental contribution to the bandpass, integrated over all channels per polarization, shall be stable to 0.3% amplitude and $0.09°$ phase for 18 m antennas, and 0.7% amplitude and $0.2°$ phase for 6 m antennas, over hourly and monthly timescales.	SYS1501, SYS6103
Calibration Database: Bandpass	CAL0504	The observatory shall supply bandpasses satisfying CAL0502 and CAL0503 in a calibration database, updating solutions where appropriate (e.g. if the advertised accuracy is no longer satisfied due to slow degradation over time or a step change arising from antenna maintenance).	SYS0703, CAL0501
Proposal Content: Estimated Dynamic Range Per Channel	CAL0505	Spectral line proposals shall specify the required dynamic range in a single spectral channel. This shall be used by the observatory to decide if the default bandpass calibration procedure is suitable or if custom bandpass calibration is required (note that an 'enhanced' bandpass calibration procedure may yet need to be defined, depending on the outcome of future investigations).	SYS1061, CAL0501

The analog and digital electronics will impose an instrumental spectral imprint on an astronomical signal. The troposphere and ionosphere will also contribute to this imprint. These effects must be measured and removed. The exact shape of the bandpass is not of key importance, as long as it is stable and can accommodate high spectral dynamic range. SYS6106 calls for 50 dB spectral dynamic range to enable imaging in the presence of bright emission lines, with particular focus in the frequency range 16–50 GHz and angular scales less than 10″. SYS6106 is therefore only relevant for MA observations (the resolution of the longest 60 m baseline of the SBA at 50 GHz is 20″). The spectral resolution assumption in Section 5.1 calls for this dynamic range to be supported for channels as narrow as 0.1 km/s (5 kHz at 16 GHz, or 17 kHz at 50 GHz). SYS6105 calls for 40 dB spectral dynamic range in absorption within 2 MHz of 1.4 GHz.

To improve observing efficiency (SYS1066), CAL0501 defines a default bandpass calibration procedure that minimizes overheads by utilizing observatory-supplied bandpasses accessed from a calibration database (SYS1063). These cataloged bandpasses need to be supplied with sufficient accuracy to support the majority of anticipated Standard Observing Mode spectral line projects. Support for SYS6106 (50 dB spectral dynamic range) can be provided without requiring per-antenna per-polarization per-channel amplitude accuracy anywhere near 0.1% (-28 dB) for $N = 107$ MA antennas. A more reasonable target for per-antenna per-polarization per-channel bandpass amplitude accuracy is $\Delta s = 1\%$ for 18 m antennas. This target is not strongly constrained, though the calculation below indicates significant challenges in delivering greater accuracy due to higher signal to noise requirements (at which point atmospheric and pointing limitations will arise). The corresponding requirement on bandpass phase accuracy is half this [RD03], namely $0.3°$. The accuracy in the bandpass is given by

$$\Delta s = \frac{\sigma_{cal}}{S_{cal}} \sqrt{2N} \ , \tag{17}$$

where S_{cal} is the flux density of the bandpass calibrator, σ_{cal} is the array sensitivity (all baselines) for the bandpass calibrator observation, and the factor of 2 represents statistically-independent bandpasses for each polarization on N antennas. To achieve $\Delta s = 1\%$ with $N = 107$ MA antennas, the signal to noise on the bandpass calibrator must be 1500 (32 dB). The anticipated thermal noise of the ngVLA using 107×18 m antennas over a 30 min integration in a 0.1 km/s channel is approximately 0.8 mJy/beam in the frequency range between 16–50 GHz. A 30 min integration is selected here because it may be necessary to quickly recalibrate an antenna following maintenance, e.g. following replacement of a front end package. This could be achieved using regular brief service-mode observations of bright calibrators with the full array, e.g. in between science blocks (note similar need in Section 5.4.2). Alternatively, if a longer timescale between maintenance and reintegration into the array is acceptable, such as 1 week or 1 month (this will depend on the anticipated fraction of out-of-service antennas in any week or month), then bandpasses can be recalibrated during these windows using longer integration times and in turn fainter sources. Accepting here the worst-case 30 min timescale (per band per maximum number of concurrently observed 0.1 km/s channels), a calibrator with flux density $S_{cal} > 1.2$ Jy will therefore be required for bandpass calibration. While demanding, this should not be problematic.

For completeness, if it were required by SYS6106, the equivalent SBA accuracy would be 0.03% for $N = 19$ antennas. If instead a reasonable target of $\Delta s = 10\%$ were selected (phase accuracy $3°$), this would demand a signal to noise of 62 on the bandpass calibrator. Taking the anticipated thermal noise of approximately 25 mJy/beam for 19×6 m antennas over a 1 hour integration within a 0.1 km/s channel in the frequency range between 16–50 GHz, a calibrator with flux density $S_{cal} > 1.6$ Jy is required. This is more demanding to meet than the equivalent requirement above for 18 m antennas. While not strictly required to satisfy SYS6106, it is set here as a goal.

CAL0502 calls for these accuracies to be maintained within 0.1 km/s channels across all ngVLA frequency space. The various filter responses (baseband, subband) will need to be taken into account in order to average these 0.1 km/s solutions to improve accuracies when using broader channel widths. The calibrations for delay and amplitude described in the previous sections will need to be applied to the data prior to bandpass measurement, so as to remove systematics associated with the troposphere (differential opacity across band) and ionosphere (phase change $\propto 1/\nu$ across band); i.e. bandpasses stored in the calibration database should only contain the instrumental contribution described at the start of this section. It is expected (following earlier calculations) that there will be sufficient accuracy in the delay and amplitude calibrations to remove the atmospheric contributions to the bandpass to well within the target accuracies above. However, this expectation should be subjected to further scrutiny in future investigations. When applying the cataloged bandpasses under the default calibration procedure (CAL0501), the effects of the atmosphere should again be taken into account using other portions of the calibration workflow.

For reference, the dynamic range limit within a single spectral channel which is limited by errors in continuum subtraction caused by bandpass errors is given by

$$D_s \approx S_{line} \left(\frac{\Delta s}{\sqrt{2N}} \, S_{cont} \right)^{-1} \quad , \tag{18}$$

where S_{line} is the flux density of the peak of the line and S_{cont} is the continuum flux density of the source. Assuming for illustration $S_{line} = 0.1$ mJy/beam, $S_{cont} = 10$ mJy/beam, $N = 107$ MA antennas, and $\Delta s = 1\%$, the channel dynamic range will be $D_s \approx 12$ dB. To improve this dynamic range, greater accuracy in the bandpass will be required. This calculation suggests that either the cataloged bandpasses will require greater accuracy than $\Delta s = 1\%$ to support a wider range of plausible observational scenarios, or instead it may argue for the creation of an 'enhanced' bandpass calibration procedure in which justified proposals can request suitable observations of a bandpass calibrator. Further work is required to compare these alternatives and, if necessary, refine the proposed calibration procedures and requirements (noting as earlier that atmospheric and pointing limitations combined with practical observing time limitations will ultimately prevent significantly improved accuracy beyond $\Delta s = 1\%$ for even wide channel widths). To ensure optimal scheduling, and in anticipation of a decision regarding the options above, CAL0505 requires the proposal process to capture the estimated dynamic range per spectral channel so that a decision can be made as to whether the observatory should supply a more accurate bandpass at the frequency of interest (eventually building up more accurate bandpasses across the full frequency space), or whether custom bandpass calibration procedures should be included in the scheduling blocks for that particular project.

Bandpasses must be stable on short timescales to prevent errors caused by effective amplitude variations (resulting in reduced spectral line and image dynamic ranges) and stable on long timescales to enable reuse of solutions from the calibration database (to optimize observing efficiency). To ensure that systematic errors in bandpass amplitudes (i.e. a systematic offset for all channels across a bandpass) do not limit image dynamic range to less than 50 dB for 107×18 m antennas and 40 dB for 19×6 m antennas (SYS6103, also SYS1501), bandpass amplitudes integrated over all channels must be stable to within 0.3% and 0.7%, respectively, over 1 hour timescales, calculated using Equation 16 assuming a 3.5 hour observation for the 18 m antennas and a 7 hour observation for the 6 m antennas (following

Section 5.3.1.1). The corresponding requirements on phase are half these values [RD03], namely $0.09°$ and $0.2°$, respectively. These requirements extend to 1 month timescales (or ideally much longer) so as to minimize the frequency of bandpass recalibration and maximize observing efficiency.

5.6 Polarization

Parameter	Req. #	Value	Traceability
Feed Basis	CAL0601	All 6 m and 18 m antennas shall be equipped with dual orthogonal linear feeds in all frequency bands. In each band, all feeds over the array shall be nominally aligned to a common specified orientation with respect to the sky frame (e.g. X feed aligned at specified angle $0°$ from the meridian at zero parallactic angle).	SYS2601, SYS1061, SYS1065
Default Polarization Calibration	CAL0602	Default polarization calibration shall apply leakages from a calibration database and measure crosshand bandpass phases using the instrumental noise diodes, without including polarization calibration scans in science observation scheduling blocks, nor using calibrators from the data to measure polarization parameters.	SYS0703, SYS1063, SYS1061, SYS1065, CAL0601

Parameter	Req. #	Value	Traceability
Polarization Leakage Accuracy	CAL0603	The observatory shall measure absolute leakages within complex error modulus 10% (18 m antennas) and 40% (6 m antennas) within 10 km/s channels across all frequency space, and measure the mean level (zero-point) of circular polarization to within 0.02% (18 m antennas) and 0.2% (6 m antennas) in each band. To enable more accurate solutions to be obtained over broader channels by averaging the 10 km/s solutions, or to enable interpolation for higher spectral resolution, the 10 km/s solutions shall be measured and stored in a way that enables accountability of spectral features.	SYS1901, SYS6103, SYS6104
Polarization Leakage Stability	CAL0604	Leakages shall be stable within band-averaged leakage modulus error 0.1% for 18 m antennas and 0.6% for 6 m antennas for at least 3 months. Goal: indefinite.	SYS1063, SYS1901, SYS6103, SYS6104
Calibration Database: Polarization Leakages	CAL0605	The observatory shall supply absolute leakages satisfying CAL0603 and CAL0604 in a calibration database, updating solutions where appropriate (e.g. if the advertised accuracy is no longer satisfied due to slow degradation over time or a step change arising from antenna maintenance).	SYS0703, CAL0602

Parameter	Req. #	Value	Traceability
Calibrator Database: Polarization Calibrators	CAL0606	The observatory shall maintain a register of sources used for leakage, circular polarization, and feed alignment calibrations in a calibrator database, including their polarimetric properties. This information shall be used only for guidance, not for calibration purposes; for example to determine if they exhibit variability (in which case they should be avoided).	CAL0604
Relative Gain Amplitude Stability	CAL0607	Stability between polarization pairs shall be within 0.3% over 5 min for all 6 m and 18 m antennas.	SYS6103, SYS6104, CAL0401
Crosshand Bandpass Phase Stability	CAL0608	Noise diodes in all bands on all 6 m and 18 m antennas shall be phase matched to deliver crosshand phase error $10°$ per 10 km/s channel per second (or equivalent at a spectral resolution that samples all bandpass features).	SYS2601, SYS1061, SYS1065, SYS0601, SYS6103, SYS6104
Feed Mechanical Alignment	CAL0609	Setting shall be within $2°$ rms from target alignment for each 6 m and 18 m antenna. Goal: $1°$ rms.	SYS6103, SYS6104, CAL0601
Rotation of Feed Platform	CAL0610	Rotation shall be within $0.5°$ rms from target alignment for each 6 m and 18 m antenna under Normal environmental conditions.	SYS1061, SYS6103, SYS6104, CAL0601
Pipeline Ingestion of GPS VTEC	CAL0611	The pipeline shall ingest and make use of GPS-derived VTEC data with time resolution < 2 hour (goal: low latency data with ~ 5 min time resolution) to account for ionospheric Faraday rotation.	SYS6103, SYS6104

Parameter	Req. #	Value	Traceability
Antenna Re-Calibration Following Maintenance	CAL0612	ngVLA observing procedures shall optimize a global schedule to minimize any idle time between antenna maintenance (e.g. front end swap) and re-calibration, and in turn reintegration to the array.	SYS2303, SYS2601, SYS1061

The polarization properties of an astronomical signal will be modified by the polarimetric response of the telescope. Ionospheric Faraday rotation will also contribute toward this imprint. These effects must be measured and removed through polarimetric calibration. There are several antenna-time-frequency dependent parameters of interest: leakage, crosshand bandpass phase, and absolute alignment of linear polarization position angles. These are described below.

Polarization calibration typically requires good coverage in parallactic angle so that the astronomical source contributions which vary sinusoidally in the antenna frame can be separated from the antenna-fixed instrumental contributions. There are a range of possible polarimetric calibration strategies, each somewhat different depending on the receptor feed basis (linear, circular), and each yielding solutions with slightly different degeneracies that result in slightly different errors in calibrated data. For reference, RD15 presents a summary of interferometric radio polarization fundamentals, as well as a detailed examination of the roles of parallactic angle coverage and calibrator signal to noise in minimizing on-axis image leakage residuals and linear polarization position angle errors. RD31 presents detailed step-by-step procedures for automating a suite of polarimetric calibration strategies in the linear and circular feed bases (designed for the CASA[11] ALMA and EVLA pipelines).

The leakage terms ('dipole' terms or d-terms) describe imperfections in the on-axis polarimetric response of each feed, quantifying the degree to which each feed is sensitive to an orthogonally polarized signal (cross-talk). The imperfections can arise from telescope geometry (e.g. asymmetries in antenna illumination, feed horn, optical alignment) and electronic hardware (e.g. polarization splitter, linear to circular polarization converter if present). Leakage solutions can be 'absolute' or 'relative', depending on whether there are sufficient observational constraints to uniquely determine all real and imaginary leakage components, or whether there are two remaining unconstrained degrees of freedom [RD30]. To overcome the degeneracy in the latter case, the real and imaginary components for one feed on one antenna (typically on the bandpass/gain reference antenna) can be (arbitrarily) set to zero, yielding relative leakages for all other feeds. When sufficient constraints are available to uniquely determine all leakage components, absolute leakages will be obtained. Crosshand bandpass phase describes the relative phase between two orthogonally polarized feeds on an antenna (this can be separated into delay and phase and solved for independently in the measurement equation; for simplicity here, the term phase will strictly refer to the residual nonlinear frequency dependent part). A crosshand bandpass phase arises because the measure-

[11] https://casa.nrao.edu/

ment equation is typically refactored to the relative phase frame of the bandpass/gain reference antenna, on which the phases for both polarizations are (arbitrarily) set to zero (the crosshand bandpass phase for the reference antenna is then propagated over the array). Finally, external calibration is required to determine the absolute alignment of linear polarization in the same way that an interferometer cannot self-calibrate the absolute flux density scale. In the circular feed basis, this requires observation of a celestial source with known position angle. However, in the linear feed basis, this is not always required. Instead, position angle calibration can be satisfied by obtaining absolute leakages (or accepting larger position angle uncertainty using relative solutions) and ensuring that feeds are nominally aligned with respect to the sky frame. See RD15 (and below) for more details regarding these parameters.

Before examining ngVLA requirements related to leakage, crosshand bandpass phase, and absolute position angle in Section 5.6.3, the motivating factors behind the overall proposed polarimetric calibration strategy and related choice of hardware feed basis are described. Sections 5.6.1 and 5.6.2 will ignore the assumption of linear feeds from Section 5.1 and instead identify which of the circular, homogeneously-aligned linear, or heterogeneously-aligned linear feed bases is best suited for ngVLA design.

5.6.1 Motivating Factors for Calibration Strategy

A key requirement for ngVLA design is that polarimetric calibration overheads must be minimized (SYS1061, SYS1065). This must be satisfied regardless of whether a short or a long polarization science observation is requested, i.e. both must be supported. This effectively requires polarimetric calibration overheads (most importantly, leakages) to be decoupled from science observing blocks, for the following reasons. First, options to obtain sufficient parallactic angle coverage are problematic. For short science observing blocks, either the observing block timeframes would need to be artificially inflated, or other science blocks would need to be interrupted to enable the polarization calibrator to be viewed over a range of parallactic angle slices. This would lower observational efficiency and increase scheduling complexity, in turn arguing against such a scheme. And second, calibration using a short observation of a calibrator with known Stokes vector is also problematic. It will be onerous to maintain a database of polarization calibrators with known Stokes vectors (including 'unpolarized' calibrators). While possible, the observational overheads and complexity required to account for source variability in all frequency bands suggests that calibration schemes that require availability of such a database should be disfavored.

For completeness, potential solutions to support short polarimetric science observations are as follows, though these are not advocated here because they require calibration overheads to be included in each science observation. First, it is conceivable to perform leakage calibration using a single observation of a resolved polarized source with spatially varying and unknown (though non-zero) fractional polarization [RD30]. A second possibility is to utilize the differential parallactic angle over the array to enable calibration using a short observation of a polarized source. However, these two schemes are not generally applicable because it cannot be assumed that all standard mode science observations will require long baselines. While the long baselines could be employed for only the calibration observations, this would require interrupting likely concurrent long baseline science observations and would lead to a reduction in overall observing efficiency. A third possibility in the case of linear feeds is to provide instantaneous parallactic angle coverage over arbitrarily short baselines by (permanently) rotating the mechanical alignments for a subset of the feeds in the array [e.g. RD33]. This heterogeneously-aligned linear feed basis would enable calibration using a short observation of a polarized source. However, this is a complex and potentially costly approach because it would affect designs for the front end including cryostat sizing (or possibly rotation of the entire dewar assembly including positioner), manufacturing scalability, and maintenance. Furthermore, if the need to perform leakage calibration in a snapshot observation is removed, then the need for this additional complexity is also removed because standard calibration techniques can be performed instead (utilizing sufficient parallactic angle during observatory service time).

Instead, to improve observing efficiency (SYS1065), CAL0602 defines a default leakage calibration procedure that minimizes overheads by utilizing observatory-supplied leakages accessed from a calibration database (SYS0703). If the leakages, crosshand bandpass phase, and absolute position angle alignment can be known a priori, and if they remain stable or can be updated as needed with time, then polarimetric calibration overheads will not need to be included in any science scheduling blocks. To achieve this, observatory-managed calibration observations must ensure that sufficient time is dedicated to sampling sufficient parallactic angle coverage to yield accurate leakages. This parallactic angle coverage is needed not only to optimally separate the instrumental and source contributions, but also to provide optimal uv coverage so that resolved source structure can be accounted for in the solutions. This process must yield absolute leakages, regardless of whether circular or linear feeds are selected, to prevent dynamic range limitations at the ~ 30 dB level in polarization[12] [RD36]. A feature of the approach above is that the observatory will only need to identify a small number of ideally highly linearly fractionally polarized sources (as few as one) per frequency band to be utilized as leakage calibrators. Infrequent monitoring of these sources will be required, but only to ensure that their fractional linear polarization has not diminished below a few percent prior to any subsequent leakage re-calibrations.

5.6.2 Choice of Feed Basis

The details of how to implement the strategy above, including effects on overall observing efficiency, depend on the choice of polarization feed basis. Having dispensed of the heterogeneously-aligned linear feed option above, the choice remains between circular and homogeneously-aligned linear feeds. In the following, the term ‘linear’ will assume the parallel alignment configuration. Historically there have been a number of arguments for choosing circular feeds over linear feeds (e.g. see discussion in RD30). However, (as made clear by RD30) these are based on a number of assumptions that require more careful evaluation for ngVLA, especially when considering the ideal strategy described above. First is the argument that to measure high accuracy linear or circular polarization, a circular or linear configuration,

[12] To first order in the product between d-terms and Stokes Q or U, when observing in the circular or linear feed basis, total intensity image dynamic range will be unaffected when comparing between relative and absolute leakages (cf. RD36). However, this assumes careful calibration so that gain corrections do not prevent cancellation of orthogonal d-terms.

respectively, is desirable. However, for telescopes with good gain stability (as is required for the ngVLA; see in particular Section 5.4), the distinction becomes negligible. A concern in the linear basis might be that the switched power system at low frequencies could become corrupted by RFI (albeit unlikely given that it would need to mimic slow parallactic angle rotation of a polarized source), but this can be addressed by suitable RFI mitigation (CAL0406). Second, a similar concern is sometimes raised regarding the (in-)ability to self-calibrate calibrated total intensity data in the linear basis, due to the need to incorporate knowledge of the target's linear polarization properties (though note that this issue is not strictly relevant here because, following Section 5.1, this document purposely seeks solutions that do not require self-calibration to meet ngVLA performance requirements). There are of course two solutions: iterate using polarization-independent gains (CASA 'T' gains) so that the (slightly incorrect) polarization and leakage contributions in the parallel hands will be mostly canceled (consider $V_{XX}+V_{YY}$ in equations below), or perform full-polarization self-calibration. Third, polarimetric calibration procedures are often simpler in the circular feed basis, but this is only true if relative leakages are acceptable. It is not true if absolute leakages are desired (e.g. see overheads in RD34), as required for ngVLA (see above). Finally, consider absolute position angle calibration. In the circular feed basis, a calibrator with known position angle must be observed. However, this will likely present a challenge for ngVLA because a source model (or set of models for a small number of sources) will need to be measured (and presumably maintained) to ensure that resolved source structure is properly accounted for over the large range of array baseline lengths. While not impossible (especially if motivated as a dedicated observatory deliverable; consider RD35 as a starting point, combined with common VLBI procedures), an easier alternative is provided in the linear feed basis. There, the need for celestial position angle calibration can be simplified if all feeds are aligned to the sky within some mechanical alignment tolerance (e.g. X nominally aligned at a specified angle[13] from the meridian at zero parallactic angle). As with the circular basis, a linearly polarized source will be required to measure the crosshand bandpass phase, but unlike the circular basis, the position angle of this source will not need to be known as the objective is simply to detect the phase difference between the signal paths from the two orthogonal feeds [RD30]. Indeed, because the position angle of the source does not need to be known, an instrument-generated polarization calibration signal (coherent between polarization pairs per antenna) can be used in the linear basis to determine the crosshand bandpass phase.

Therefore, from a calibration perspective for ngVLA, there are no strong arguments for ruling out circular or linear feeds, and there is a slight preference for the latter. The unbiased considerations above lend support to the setup assumed for the ngVLA Reference Design, in which all antennas (6 m and 18 m) are equipped with dual orthogonal linear feeds in all frequency bands. Given the considerations above, CAL0601 stipulates that all feeds in any given frequency band shall be oriented with the same nominal alignment against the sky frame (i.e. the homogeneously-aligned case).

The assumption of linear feeds in the ngVLA Reference Design is therefore strongly supported by the combination of calibration arguments above, the desire to access wider usable bandwidths than available from circularly polarized feeds (enabling coverage between 1.2 GHz to 116 GHz with fewer receivers),

[13] When the specified angle is 0°, the X and Y feeds may also be termed the vertical V and horizontal H feeds, respectively.

and by the desire to optimize sensitivity and reduce complexity due to lack of polarization conversion from the native linear sampling.

5.6.3 Implications

Implications for ngVLA design will be examined below, motivated by consideration of absolute leakage, crosshand bandpass phase, and absolute position angle calibrations assuming parallel linear feeds.

Following notation from RD15, the model visibilities for a single baseline (antennas indices i and j) viewed at parallactic angle ψ with crosshand phase ρ and corrupted by complex leakage d_{Ak} (indicating the fraction of orthogonal polarization B sensed by feed A on antenna k) are given by

$$V_{XX} = (\mathcal{I} + \mathcal{Q}_\psi) + \mathcal{U}_\psi \, (d_{Xi} + d^*_{Xj}) \quad (19)$$

$$V_{XY} = [(\mathcal{U}_\psi + i\,\mathcal{V}) + \mathcal{I}\,(d_{Xi} + d^*_{Yj}) - \mathcal{Q}_\psi \,(d_{Xi} - d^*_{Yj})]\, e^{i\rho} \quad (20)$$

$$V_{YX} = [(\mathcal{U}_\psi - i\,\mathcal{V}) + \mathcal{I}\,(d_{Yi} + d^*_{Xj}) + \mathcal{Q}_\psi \,(d_{Yi} - d^*_{Xj})]\, e^{-i\rho} \quad (21)$$

$$V_{YY} = (\mathcal{I} - \mathcal{Q}_\psi) + \mathcal{U}_\psi \, (d_{Yi} + d^*_{Yj}) \quad (22)$$

where Stokes $\mathcal{Q}_\psi \equiv \mathcal{Q}\cos 2\psi + \mathcal{U}\sin 2\psi$, Stokes $\mathcal{U}_\psi \equiv \mathcal{U}\cos 2\psi - \mathcal{Q}\sin 2\psi$, and terms multiplied by second order leakages (e.g. $d_{Xi}\, d^*_{Xj}$) are neglected. The terms above are frequency dependent. Antenna feeds are typically engineered with great care to be orthogonal such that $d_{Xi}+d^*_{Yi} = 0$. The approximate level of spurious post-calibration linear ($\mathcal{L}_\epsilon$) or circular ($\mathcal{V}_\epsilon$) polarization for an on-axis target with total flux density $\mathcal{I}$ is given by

$$\frac{\mathcal{L}_\epsilon}{\mathcal{I}} \approx \frac{\mathcal{V}_\epsilon}{\mathcal{I}} \approx \frac{\sigma_d}{\sqrt{N}} \approx \frac{\sigma_{dc}}{\sqrt{N N_c}} \ , \quad (23)$$

where N is the number of antennas in the array, and $\sigma_d = \sigma_{dc}/\sqrt{N_c}$ is the real-valued magnitude of the residual complex error for one polarization on one antenna after band-averaging channelized complex leakage errors with typical magnitude σ_{dc} over N_c channels [RD15]. This equation implicitly assumes $M = 1$ (see notation from RD03), namely that leakages are constant throughout the observation (examined further below).

SYS1901 and SYS6104 call for 35 dB brightness dynamic range on-axis in a continuum image of linear or circular polarization at 8 GHz, and 25 dB over wide-field mosaics at 27 GHz. SYS6103 calls for 45 dB brightness dynamic range on-axis in total intensity at 8 GHz, and 35 dB over wide-field mosaics at 27 GHz. These requirements place constraints on d-term accuracy. (Note that wide-field polarization effects were addressed earlier in Section 5.2.2.) Assuming conservatively $N_c = 5000$ channels across a frequency band (e.g. $\sim$ 2 GHz bandwidth in band 2 at 10 km/s resolution; note that the edge $\sim 10\%$ of channels in any band will likely exhibit degraded performance) with $N = 107$ MA antennas, channelized $\sigma_{dc} = 10\%$ ($\sigma_d = 0.1\%$) is required to attain 39 dB image dynamic range in linear or circular polarization. This will also be sufficient to satisfy SYS6103; -39 dB residual leakage from Stokes I

to linear polarization implies that, for targets with $\sim 10\%$ linear polarization (approximate upper limit relevant for extragalactic sources in SYS6103 deep field studies), residual leakage from linear polarization to Stokes I will be below -49 dB (e.g. consider forming Stokes I from Equations 19 and 22). Performing the equivalent calculation for $N = 19$ SBA antennas yields a requirement for channelized $\sigma_{dc} = 40\%$ ($\sigma_d = 0.6\%$) to attain 29 dB image dynamic range in linear or circular polarization.

Absolute leakages are necessary for two key reasons. First, as motivated earlier, they are required to facilitate high dynamic range imaging. If relative leakages are obtained, the unknown real and imaginary d-term offsets will limit image dynamic range[14] to ~ 30 dB in polarization [RD36]. For example, the polarization limit can be crudely estimated by considering amplitude errors arising from corruption of Equation 20. Assuming 2% band-averaged leakages[15] per polarization per antenna, in which case the relative real offset over the array will be $\sim 2\%$, and assuming a 5% linearly polarized target, the polarimetric dynamic range will be limited to $1/(0.02 \times 0.05) \approx 30$ dB. For 5% band-averaged leakages and an 8% linearly polarized target this could even be as low as ~ 24 dB. And second, absolute leakages are required to set the zero-point for circular polarization. If relative leakages are obtained, the unknown imaginary component of the d-term on the reference antenna's X feed (arbitrarily set to zero in CASA, and propagated over the array) will translate to an unknown offset in circular polarization. External calibration is required to determine this offset, in the same way that an interferometer cannot self-calibrate the absolute flux density scale. Ideally this would be accomplished using an observation of an absolute circularly polarized flux density calibrator. However, no such sources are known. Rather than attempt to identify and monitor such sources, an alternative is to apply a statistical constraint by observing a sample of circularly polarized sources (per frequency band) and assuming that the Universe has no preferred handedness for circular polarization [e.g. RD32]. If this is the case (or, if not, assuming that any systematic handedness is at a level below the accuracy required here for the imaginary leakage component), then the imaginary component can be set by the mean level (zero-point) of circular polarization over the sample. The required accuracy in band-averaged imaginary leakage offset is 0.02% to yield unbiased 37 dB circular polarization dynamic range, or 0.2% to yield 27 dB. Therefore, a sample of at least ~ 25 sources exhibiting $\sim 0.1\%$ fractional circular polarization (typical level for sources investigated by RD32) will be required to yield an uncertainty in their mean (zero-point) of 0.02%. This is feasible for an observatory program.

For completeness, it should be noted that absolute leakages will deliver more accurate absolute position angle alignment than relative leakages, although unlike above this is not a key motivation for seeking absolute leakages. If relative leakages are obtained, the unknown real component of the d-term on the reference antenna's X feed (arbitrarily set to zero in CASA, and propagated over the array) will translate to an unknown offset in absolute position angle given by the magnitude of the true $\mathrm{Re}(d_{X,\mathrm{ref}})$

[14] Strictly, as discussed by RD36, there are circumstances in which dynamic range will not be limited, but rather fidelity (i.e. a systematic difference between the reconstructed and true sky). Absolute leakages are therefore further motivated by the desire to avoid such subtleties between the types of errors incurred.

[15] If channelized leakage amplitudes are 2% and there are minimal frequency-dependent variations in leakage phase across the band, then the band-averaged systematic leakage will be of the same magnitude.

[e.g. RD15]. For example, assuming 2% band-averaged leakages, the resulting absolute position angle uncertainty when using relative leakage solutions will be $\sim 1^\circ$. This is unlikely to be significant for scientific position angle measurements. This error will be systematic for any given observation. Changes in absolute position angle alignments between observations in a multi-epoch dataset will degrade polarimetric image dynamic to ~ 30 dB (see calculation below assuming $\Delta\theta = 1^\circ$ and neglecting the factor $1/\sqrt{N}$), though this can be mitigated in software by ensuring that the selected reference antenna is available in each observation. However, whether relative or absolute leakages are recovered, accuracy in the d-term solutions for each epoch will also produce differences in absolute position angle alignment between epochs. To illustrate, consider effective gain errors in Stokes U that will lead to degraded polarimetric dynamic range. Assuming fractional linear polarization $L/I = \sqrt{Q^2+U^2}/I = 5\%$ where $\vec{L} = Q + iU = Le^{i2\theta}$ with position angle θ, observations at zero parallactic angle and nominal Stokes $U = 0$ without loss of generality, $\sigma_d = 0.1\%$ (as above), $N = 107$ MA antennas, and absolute position angle variation between observations $\Delta\theta = 0.006^\circ$ arising from systematic offset $\sigma_d/\sqrt{N} = 0.01\%$, variations in Stokes U in the combined dataset will be $\Delta U/I = \sin(2\Delta\theta)\,L/I = 0.001\%$. Assuming these differences are randomized over at least 2 observations (following Section 5.3.1.1), the effective dynamic range limit in linear polarization will be ~ 52 dB. Performing the equivalent calculation for $N = 19$ SBA antennas with $\sigma_d = 0.6\%$, the dynamic range limit will be ~ 40 dB. These levels exceed the requirements from SYS6104.

An additional systematic position angle offset will be present, even if absolute leakages are obtained, even if these leakages are known with zero error, and indeed even if these leakages are identically zero, because each antenna in the array will exhibit a nonzero error in mechanical feed alignment about their design orientation (i.e. even if the dipoles on any given antenna are perfectly aligned with respect to each other, they may be misaligned with respect to a neighbouring antenna; antenna leakages are antenna-based and do not capture this information). This will lead to an offset between the assumed and true sky frames. In principal, external absolute position angle calibration is required to account for this offset. However, if mechanical offsets are sufficiently small, then external position angle calibration will be unnecessary. From an engineering perspective, it is very difficult (and therefore costly) to set the alignment of each feed to better than 1° rms. An uncertainty of 2° rms is considered to be a reasonable target (e.g. as demonstrated by ALMA; RD38). For an array with $N = 107$ MA antennas, 2° rms implies a systematic position angle offset of 0.2°. For $N = 19$ SBA antennas the systematic position angle offset is 0.5°. These values exceed any reasonable scientific expectations for position angle accuracy. However, differences in feed alignments across the array will also produce gain errors that will limit image dynamic range. Following notation from RD15, incorporating characteristic difference $\alpha = \sqrt{2}\beta$ in the otherwise common parallactic angles viewed by two antennas over a baseline where β is the rms feed alignment uncertainty per antenna, ignoring leakages, and assuming (without loss of generality) observation at zero parallactic angle, the relationships between the four reconstructed Stokes parameters (primed) and the Stokes parameters that would be measured from ideal visibilities (unprimed) are given by[16]

$$I' = I\cos\alpha - iV\sin\alpha \tag{24}$$

[16] See also RD37 for a derivation of these equations, though note errors in sign and in the interpretations of the equations.

$$Q' = Q\cos\alpha + U\sin\alpha \quad (25)$$
$$U' = U\cos\alpha - Q\sin\alpha \quad (26)$$
$$V' = V\cos\alpha - iI\sin\alpha \;. \quad (27)$$

The effects are as follows. Amplitude calibration will offset antenna-based gains by mean $\cos\alpha$, but the scatter in these solutions will yield antenna-based gain errors[17] $(1-\cos\beta)$ that will limit image dynamic range to approximately $N/(1-\cos\beta) \approx 52$ dB (using Equation 1) for $\beta = 2^\circ$ and $N = 107$ MA antennas. This limit is 45 dB for $N = 19$ SBA antennas. Equations 25 and 26 indicate that linearly polarized intensity will be unaffected (i.e. $L' = \sqrt{(Q')^2 + (U')^2} = L$). Similarly, the mean polarization position angle over all baselines will be unaffected, though position angles measured along all baselines to any given antenna will exhibit scatter with magnitude[18] $\beta/2$. This scatter will lead to errors in linear polarization entering Equations 19–22 and in turn degrade image dynamic range in all Stokes parameters. A worst-case dynamic range limit can be estimated using the relationship for $\Delta L/I$ above and assuming a target with fractional linear polarization $\sim 10\%$, giving $N/(L/I \times \sin\beta) \approx 45$ dB for $\beta = 2^\circ$ and $N = 107$ MA antennas. This limit is 37 dB for $N = 19$ SBA antennas. Feed alignment errors must ideally be within 1° to deliver 49 dB and 40 dB for the MA and SBA, respectively, and in turn satisfy SYS1501 and SYS6103. Finally, Equation 27 indicates that $I\sin\alpha$ will contaminate the real part of the cross-hand visibilities (Equations 20 and 21), namely linear polarization (Stokes V will be unaffected), with zero systematic mean offset (due to the odd function of $\sin\alpha$) and non-zero scatter. The scatter will yield effective antenna-based gain errors that will lead to dynamic range limitations when imaging linear polarization. These gain errors can be estimated by $N/(\sin\beta) \approx 35$ dB for $\beta = 2^\circ$ and $N = 107$ MA antennas. The limit is 27 dB for $N = 19$ SBA antennas. Feed alignment errors must ideally be within 1° to deliver 38 dB and 30 dB for the MA and SBA, respectively, and in turn satisfy SYS6104.

It is not clear how feasible it is (economically, mechanically, and accounting for factors like on-site maintenance timeframes) to deliver mechanical feed alignment accuracy within $\beta = 1^\circ$ rms. However, this can be accomplished using celestial calibration. Engineering mechanical feed alignment can then be relaxed to a realistic target of 2° rms (or perhaps even larger if the cost penalty is high). Feed alignment calibration requires a linearly polarized source with antenna-based SNR $(2\beta)^{-1} \approx 15$ dB (RD07 Equation 9.67 with factor 2 for position angles). Assuming a target calibrator with fractional linear polarization no less than 3%, this implies a calibrator with antenna-based total intensity SNR 30 dB. The sensitivity of the ngVLA is anticipated to be no worse than 12 μJy/beam when using $N = 107$ MA antennas in a 5 min period in any band and conservatively assuming only 50% of the maximum observable bandwidth. A calibrator with total flux density greater than 80 mJy is therefore required. For $N = 19$ SBA antennas the equivalent sensitivity is 0.4 mJy/beam, yielding a calibrator flux density requirement of 1.7 Jy (or less for a longer observation). This approach is therefore realistic. The absolute position angle of the calibrator does not need to be known. However, the calibrator must be spatially unresolved on all baseline lengths of interest so that they all see the same position angle. This may be challenging

[17] Gain errors scale with β rather than α because the former is the typical misalignment that an antenna will see against the average misalignment from all other antennas (i.e. against $\beta/\sqrt{N-1} \approx 0^\circ$).

[18] The factor of 2 arises because position angles are periodic in 180°.

to ensure over long baselines; however, this can be overcome by specifying a maximum baseline length for the calibration and extending the time period for the observation accordingly. Calibrators exhibiting variability over hourly timescales must be avoided.

Feed alignments must remain stable indefinitely, accommodating in particular any quasi-static systematic antenna deformations (e.g. thermal deformation) that could lead to systematic rotation in the feed platform. It is reasonable to expect (and to formally require) that this will be satisfied by antenna design, which must support blind pointing under normal conditions within 0.01° for 18 m antennas and 0.03° for 18 m antennas (CAL0201). Note the alternative: if feed alignment stability cannot be maintained, calibration will need to be performed regularly during science observations (e.g. tracking antenna deformations sampled by offset pointing calibration), resulting in an unacceptable decrease in observing efficiency (SYS1061). Short-term instability may be acceptable as long as it integrates down to within 1° over the time period of interest (e.g. wind loading, and perhaps sunrise/sunset where differential heating/cooling may temporarily 'inflate'/'deflate' the structure in an unpredictable manner before settling within a steady state). CAL0610 highlights this issue in a formal requirement, targeting 0.5° rms (half the feed alignment goal).

The absolute leakages will need to be supplied to science observations through a calibration database, with sufficient spectral resolution to support Standard Observing Mode projects. There are no requirements on this spectral resolution, so 10 km/s over all ngVLA frequency space will be assumed (33 kHz at 1 GHz, 3.3 MHz at 100 GHz); this may be subject to change in the future. The various filter responses (baseband, subband) will need to be taken into account so that stored solutions can be averaged as required to supply science observations with channel widths greater than 10 km/s. Such averaging will also improve leakage accuracy, but only down to the level of atmospheric and pointing limitations associated with the leakage calibrator observations. Interpolation may be used to support narrower widths. Should these derived products be insufficient for some Standard Observing Mode projects, it may be necessary to consider the creation of 'enhanced' polarization calibration procedures in which justified proposals can request suitable observations of polarimetric calibrators.

To deliver leakage amplitude accuracy $\sigma_{dc} = 10\%$ per channel with $N = 107$ MA antennas, the array signal to noise on the leakage calibrator must be $\sqrt{2N}/\sigma_{dc} \approx 150$ (22 dB). The thermal noise is anticipated to be no worse than 0.8 mJy/beam within a 10 km/s channel when using 107×18 m antennas in a 2 min period in any band. A calibrator with flux density $S_{cal} > 0.1$ Jy will therefore be required for leakage calibration. Similarly, to deliver $\sigma_{dc} = 40\%$ for with $N = 19$ SBA antennas, the array signal to noise must be ~ 12 dB. Taking worst-case sensitivity 40 mJy/beam within a 10 km/s channel when using 19×6 m antennas in a 2 min period in any band, the requirement is $S_{cal} > 0.6$ Jy. These calibrations will not be problematic.

Additional requirements for the observatory-managed procedure to measure absolute leakages are as follows. Only (ideally strongly) linearly polarized calibrators can be accepted for absolute leakage calibration; position angle calibration (solving for the real component of the d-term on the reference feed) cannot be performed with an unpolarized source (as intuitively expected). Selected leakage calibrators must contain a compact polarized component that is detectable over all baseline lengths. Any selected leakage calibrator must be observed with sufficiently wide parallactic angle coverage so that intrinsic source structure (i.e. baseline dependence) will be taken into account in the solutions (similar to CAL0702). It will be necessary to account for (and ideally utilize for improved constraints) differential parallactic angle coverage over long baselines and the likely resolved fractional polarization structure of calibrators (see related comments in Section 5.6.1). To enable efficient calibration over all frequency space, 2 min integration time per bandwidth range (as above) can be interleaved over a multi-hour observing block. This will also need to include a circular polarization calibrator survey (as above). Care will need to be taken to account for, or avoid, sources that exhibit variability on short timescales, possibly minutes (e.g. see the polarimetric intraday variable in Figure 2 in RD32); variability on timescales associated with gathering parallactic angle coverage (hours) may be prevalent in the bright source population used to measure leakages and circular polarization. Polarization properties of leakage and circular polarization calibrators should be stored in a calibrator database, though only for the purpose of identifying variability (and thus potentially avoiding them in the future; see also comment at end of Section 5.6.1); quantitative details from these records should not be used when obtaining any new calibration solutions. Stability requirements for leakage solutions are addressed futher below.

The leakage solutions will be affected by Faraday rotation in the lower frequency bands. When linearly polarized radiation traverses a birefringent medium such as a magnetized thermal plasma, it will undergo Faraday rotation, resulting in a rotation of the position angle of linear polarization. The rotation arising from signal passage through the plasmasphere and ionosphere (dominated by the latter; see Section 5.3.1.2) is given by

$$\Delta\theta_f = \frac{e\,c\,r_0}{2\pi m_e \nu^2}\int B_{los}(l)\,n_e(l)\,dl \tag{28}$$

$$\approx \frac{1.35}{\nu^2}\,B_{los}\,N_e \;\; \mathrm{deg} \;\; , \tag{29}$$

where e is the electron charge, c is the speed of light, r_0 is the classical electron radius, and m_e is the electron mass. The approximation in Equation 29 is for a thin shell ionized atmosphere with representative line of sight magnetic field B_{los} in units of gauss (positive when pointed toward the observer, and which can be suitably estimated by taking the Earth's $B_{los}(l)$ at the height of the weighted-column thin-shell; RD18), where ν is the observing frequency in units of GHz and N_e is the STEC in units of TECU (recall definitions from Equation 11). Alternatively, Equation 29 can be written in terms of rotation measure,

$$RM \approx 0.26\,B_{los}\,N_e \;\; \mathrm{rad/m^2} \;\; . \tag{30}$$

The STEC above each antenna can be estimated by combining GPS-derived VTEC maps, available from external sources such as the IGS, with a model of the Earth's magnetic field, such as that provided by the International Geomagnetic Reference Field (IGRF). The IGS 'Final' maps aggregate results from several analysis centers worldwide with 2 hour time resolution that are published with ~ 2 week latency. The

Jet Propulsion Laboratory (JPL) Global Differential GPS System (GDGPS[19]) publishes real-time VTEC maps every 5 mins. Similarly, the Massachusetts Institute of Technology (MIT) Automated Processing of GPS (MAPGPS[20]) service publishes VTEC maps every 5 mins, but these differ from the sources above in that data are only provided along slightlines where satellites were present rather than interpolating to produce standardized TEC maps that are regularly sampled in latitude and longitude. Diurnal variations in VTEC at the VLA site typically range from a maximum of ~ 50 TECU to a third of this value at night (with further modulation from various dynamics highlighted in Section 5.3.1.2). STEC values rise with increasing zenith angle to within factor 5, or ~ 250 TECU, at $\sim 80°$. VTEC data such as that provided by the IGS typically exhibit uncertainties within ~ 2 TECU (best-case ~ 1 TECU, worst-case ~ 5 TECU). STEC uncertainties are then typically within ~ 10 TECU. The Earth's line of sight magnetic field at the VLA site ranges between 0 G to $+0.4$ G with typical value $+0.2$ G over the sky at the IGS-assumed 450km height of the thin-shell ionosphere [RD18]. The equations above indicate that changes in STEC and B_{los} throughout a long observation could lead to antenna-based variations as large as ~ 20 rad/m^2 in rotation measure, or equivalently $\sim 2°$ in position angle when observing at 8 GHz (band 2, relevant for SYS6103 and SYS6104). If GPS-derived VTEC data with 10 TECU STEC uncertainties are used to remove these variations when calibrating the telescope data, the residual errors could be as large as 1 rad/m^2, or respectively $0.4°$ and $0.04°$ at the lower (3.5 GHz) and upper (12.3 GHz) ends of band 2.

Variability in ionospheric Faraday rotation will cause position angles to be rotated above each antenna as a function of time, leading to scatter in Stokes Q and U and in turn degrading image dynamic range in all Stokes parameters. This is analogous to feed misalignment errors described earlier, characterized by Equations 25 and 26. The dynamic range limit arising from antenna-based rms fluctuations in position angle γ is then given by $N\sqrt{M}/(L/I \times \sin\gamma)$ where M is the number of statistically independent samples throughout the observation. This implies worst-case $\gamma < 2°$ (or less if the effective N needs to be reduced to account for correlated ionospheres overhead) to satisfy the 45 dB total intensity imaging requirement from SYS6103 (and automatically the 35 dB polarization imaging requirement from SYS6104), assuming $N = 107$ MA antennas, a target with 10% fractional linear polarization, and worst-case $M = 2$ for a 4 hour observation (following Section 5.3.1.1) over which the ionosphere varies with 2 hour coherence timescale. This is at approximately the same level as described earlier for the ionosphere and suggests that, to satisfy SYS6103 and SYS6104, the ngVLA data reduction pipeline will need to ingest VTEC data to correct for ionospheric Faraday rotation. The need for $\gamma < 2°$ also suggests that the typical ~ 2 TECU accuracy of external GPS-derived VTEC data will be sufficient to satisfy SYS6103 and SYS6104; ionospheric Faraday rotation will not need to be measured using array observations of polarized calibrators, in turn avoiding the need for calibrator polarization selection criteria and associated monitoring and database overheads. VTEC data with 2 hour time resolution should provide sufficient accuracy over the interpolation period. However, VTEC data with low latency at 5 min time resolution (e.g. GDGPS or MAPGPS, latter with improved spatial resolution) is ideally required in order to minimize deviations between the true STEC values and the GPS-derived model, and more importantly to eliminate complications (and associated costs) for ngVLA data reduction scheduling that would arise from the

[19] http://www.gdgps.net/products/tec-maps.html
[20] https://www.haystack.mit.edu/atm/arrays/gps/index.html

need to accommodate the 2 week latency of the IGS data. Careful commissioning will be required to ensure that any systematic biases in the ingested VTEC data are identified and removed, for example by comparing VTEC data with band 1 observations of a calibrator with known position angle (e.g. 3C286); it is known that there are systematic differences (~ 2 TECU) between the IGS, GDGPS, and MAPGPS reconstructed VTEC values. Finally, note that errors of 1 rad/m^2 arising from STEC uncertainties of 10 TECU imply position angle errors $\sim 4^\circ$ at 1.2 GHz. Following the calculation above, this will result in a dynamic range limit in total intensity of ~ 43 dB. Celestial calibration may help to improve this limit (note also the similar 42 dB limit at 1.2 GHz arising from upper-limit ionospheric phase calibration, from Equation 13). Equivalent calculations to those presented above are not performed for the SBA because the relevant image dynamic range requirements are specified at 27 GHz where the effects of the ionosphere are negligible.

If the true leakages are sufficiently stable with time, then calibration database solutions will remain valid for an extended period of time and re-calibration overheads can be minimized (SYS1063, SYS1065). Ideally, leakages should only need to be measured once, with results valid for years, or at minimum over the time period between antenna/receiver maintenance. Leakage solutions are expected to be stable with time because their origins are rooted in antenna and feed geometry (and good engineering). Variations arising from antenna deformation (e.g. differential heating, which gives rise to the need for offset pointing) or elevation changes (e.g. changing aperture illumination) are not expected to be significant within the leakage accuracy required here (systematic $\sigma_d = 0.1\%$ for 18 m antennas and $\sigma_d = 0.6\%$ for 6 m antennas). CAL0604 states this in a formal requirement. This stability will need to be demonstrated during the ngVLA commissioning phase. RD39 found that leakages on the Very Long Baseline Array (VLBA) were stable over a period of 16 months. Similarly, RD40 examined calibration stability for the Jansky Very Large Array (JVLA) at L-band over a period of 5.5 years, finding that leakages for each antenna remained stable over multiple years unless affected by a receiver change.

Some forms of antenna maintenance, and particularly changes in an antenna's front end package, will result in new leakages for that antenna. When such events occur, the leakages (and other antenna-based calibration parameters) will need to be recalibrated. Several antennas may be serviced in any given week. A detailed service-mode calibration schedule will need to be developed to optimize the approach for re-calibrating these antennas and returning them to science observations (including ensuring compatibility with the needs of other calibrations like absolute amplitude and bandpass; recall Sections 5.4.2 and 5.5). For example, the highest overall efficiency may be achieved by targeting front end replacements early in the week followed by a weekly 'calibration day', even if this means that one or two antennas could remain idle for up to a few days. A multi-hour (e.g. 10 hour) calibration run (which may not require the full array) could be performed every Wednesday with the aim to (automatically) process the data overnight and subsequently (semi-automatically) assess the results and update the calibration database on Thursday. This would provide regularity for personnel, and sufficient observing time to ensure that factors such as parallactic angle and frequency space can be sufficiently sampled without significantly affecting overall science observing efficiency. Alternatively, if absolute leakages can be calibrated using a very short observation (e.g. by taking into account the constraints provided by the majority of unaffected antennas with unchanged leakages), then antennas could be rapidly returned to science observations after completion of their maintenance visit.

Relative gain amplitude stability between polarization pairs on any given antenna is required to ensure that Stokes parameters and polarization calibration parameters can be accurately calculated. Stability is also required to satisfy image dynamic range limits, so that all correlation products can be calculated within the same levels of uncertainty. The requirement for crosshand gain amplitude stability (CAL0607) is therefore the same as for noise diode stability (CAL0401).

The crosshand phase frame must remain stable to prevent corruption of the recovered Stokes parameters and leakages. To maximize observing efficiency (SYS2601, SYS1061, SYS1065) and enable rapid polarization calibration (e.g. necessary for beamforming), crosshand bandpass phase calibration must be performed using an instrument-generated calibration signal rather than observations of celestial calibrators. This can be accomplished by utilizing the noise diodes provisioned in the current ngVLA design. These inject noise into the RF signal path between the feed horn and the low noise amplifiers (LNAs) in bands 1 and 2, and between the orthomode transducer (OMT) and the LNAs in the remaining bands [AD10]. The noise diodes must be phase matched so that there is zero phase difference at the coupling points. The noise diode system will not be sensitive to any crosshand phase arising upstream of the noise injection point (feed, antenna structure). Commissioning activities will need to include characterization of upstream crosshand phase over all frequency space on all antennas, for example to identify possible temperature dependence (though this is not expected to be significant as the feeds will be cryogenically cooled). This may be accomplished using a celestial calibrator observed over a wide range in parallactic angle. An alternative to the noise diode approach could be to install a pulsed harmonic comb generator [e.g. RD07 Sec. 9.5.7] in every band on every antenna. However, this would involve additional complexity and cost without providing significant benefits over the currently provisioned noise diode approach.

Crosshand phase measurement errors will behave similarly to leakage errors, leading to image dynamic range limitations (SYS6103, SYS6104). Equation 23 can therefore be rewritten as

$$\frac{\mathcal{L}_\epsilon}{\mathcal{I}} \approx \frac{\sigma_\rho}{\sqrt{M}} \approx \frac{\sigma_{\rho c}}{\sqrt{M N_c}} \ , \tag{31}$$

where $\sigma_\rho = \sigma_{\rho c}/\sqrt{N_c}$ is the residual crosshand phase error on one antenna after band-averaging statistically-independent channelized crosshand phase errors $\sigma_{\rho c}$ over N_c channels, M is the number of statistically independent time samples, and the number of antennas in the array (N) is not present (unlike Equation 23) because crosshand phase is propagated from the reference antenna over the array. For consistency with the leakage accuracy calculation presented earlier, it will be assumed here (conservatively) that $N_c = 5000$ channels of width 10 km/s are sufficient to sample all crosshand bandpass features across a frequency band. Assuming 1 second sampling with errors that will integrate down over a 5 min period (conservatively $M = 300$) so that accurate calibration may be achieved over a short observation, $\sigma_{\rho c} < 10°$ is required for 18 m antennas to satisfy the requirement from SYS6104 for 35 dB polarimetric dynamic range at 8 GHz. While the requirement for 6 m antennas is strictly

$\sigma_{\rho c} < 100^\circ$ to satisfy 25 dB polarimetric dynamic range at 27 GHz, the stricter requirement is adopted here to avoid complexity (and potentially cost) with differing hardware requirements between antennas. Therefore each noise diode should ideally deliver channelized uncertainty 10° on a ~ 1 second timescale. This calculation will need to be reassessed if any of these assumptions are inappropriate, for example if channelized phase errors will not be statistically independent.

Finally, it is worth noting that the ngVLA could offer parallel-hand only observations (XX and YY only; e.g. see L4 calibration strategy in RD31, as used by ALMA), for example to reduce data rates or trade full cross-product correlation for increased spectral resolution. The ngVLA's amplitude stability, crosshand gain stability, and database leakages could be used facilitate this strategy (see also e.g. RD41).

5.7 Calibrator Structure

Parameter	Req. #	Value	Traceability
Calibrator Search and Characterization	CAL0701	The system shall facilitate rapid (∼minutes) blind search and characterization (e.g. histogram of amplitude ratios over binned baseline lengths) of complex gain calibrators within 3° of any (accessible) sky coordinate. The system shall prioritize re-detection of promising (minimally-variable) previously known calibrators from the calibration database.	SYS3005, SYS2221, CAL0704
Modeling of Calibrator Structure	CAL0702	The system shall facilitate rapid (∼minutes) modeling of calibrator internal structure in total intensity. Goal: perform this in full polarization.	SYS3005, SYS2221
Array Configuration Snapshot Performance	CAL0703	The ngVLA antenna configuration shall be optimized to support robust snapshot calibrator modeling.	CAL0702

Parameter	Req. #	Value	Traceability
Calibrator Database: Source Ingest	CAL0704	The system shall support ingestion of new calibrator models into the calibrator database, noting that these may be time-dependent and so must be stored in a manner suitable for examining light curves and changes in source structure.	SYS1061, CAL0702

The wide range of baseline lengths proposed for the ngVLA will make it necessary to take into account the likely resolved structure of any given calibrator prior to using it for complex gain referencing or other purposes. Fortunately, the ngVLA's excellent snapshot uv coverage (arising from a rather random, non-geometric distribution of antenna locations) should enable rapid calculation of robust models of source internal structure from snapshot observations. CAL0701 requires the ability to quickly scan around a target region of sky to find a suitable calibrator. This will be of use in the automated preparation of both standard observing modes and triggered modes. CAL0702 requires the ability to rapidly derive a model of the calibrator's internal structure in total intensity, with a goal to perform this in full polarization (a side benefit of this effort will be a scientifically interesting database). CAL0703 is defined to ensure that the ability to derive a robust calibrator model from a snapshot observation is accounted for when optimizing the final fixed ngVLA antenna configuration. CAL0704 requires calibrator models to be compiled within a calibrator database so as to improve observational efficiency for future observations. Note however that this will likely only minimize the time required for calibrator search. Modeling of calibrator structure will likely need to take place every time a calibrator is used, to account for variability (particularly at higher frequencies).

5.8 Summary

5.8.1 Requirements

The key L1.1 requirements are summarized as follows. These are identified by antenna diameter where distinct. Entries without an asterisk focus on hardware characteristics (functional requirements). Entries marked with an asterisk indicate requirements that focus on measurement uncertainties (operational requirements; these require sufficient time dedicated to service mode calibration observations). Entries marked with a daggar summarize key capabilities.

Precision Pointing:	$8''/3''$ offset, $40''/15''$ blind for 6 m/18 m
Normal Pointing:	$17''/5''$ offset, $85''/25''$ blind for 6 m/18 m
Aperture Plane Error:	340 μm/800 μm rms in precision/normal conditions
Primary Beam*:	1% of boresight response in $\Delta\nu = 10$ MHz within -10 dB power contour
Motion:	Slew 3° in 7 sec including time to settle within offset pointing error
Antenna Location:	0.2 mm/0.5 mm 3D error for 6 m/18 m after removing systematic drifts
Timing Accuracy:	70 ms over 60 m with 6 m dishes, 10 μs over 1000 km with 18 m dishes
Feed Basis:	Linear feeds in all frequency bands with common alignment over array
Feed Alignment:	Setting within 2° rms of target alignment, goal of 1° rms
Polarization Leakage*:	Complex error modulus 40%/10% per 10 km/s channel for 6 m/18 m
Instrumental Bandpass*:	10%/1% per 0.1 km/s channel for 6 m/18 m, opacity corrected on use
Amplitude Stability:	Internal switched power amplitude scale tied $\leq$monthly to celestial scale
Noise Diode Stability:	0.3% drift over 5 min, 1% drift over 1 month
Tropospheric Delay:	0.1 ps drift over 5 min, 1 ps rms in 8 sec, goal of 180 fs rms in 1 sec
Ionospheric Delay:	$2/\nu_{GHz}^2$ ps drift over 5 min, $20/\nu_{GHz}^2$ ps rms in 10 sec
Delay Stability:	Tropo: IADCS on 244×18 m and $\geq 2 \times 6$ m; Ion: frequency switching
Crosshand Stability:	Amplitude: Switched power; Phase: Phase-matched noise diodes
Antenna Delay:	60 fs drift over 5 min across 3° on sky, 100 fs rms in 1 sec
Electronic Delay:	80 fs drift over 5 min across 3° on sky, 70 fs rms in 1 sec, per pol.
Calibration Overheads:	Observatory maintained calibration database for maximal efficiency
Automation:	Fully automated scheduling and pipeline processing for standard modes
Polarimetry†:	Full Stokes and snapshot polarimetry supported
Amplitude†:	Absolute flux density accuracy 1% best-case, goal of 6% worst-case
Dynamic Range†:	45/35 dB image at 8/27 GHz, 35/25 dB in polarization, 50 dB spectral

5.8.2 Error Comparison

The following tables present comparisons between different sources of instrumental error per-antenna within a standardized observation duration of 1 sec. Error contributions have been derived from the requirements presented in this document. Conversions from the values specified in the requirements have been performed where appropriate, for example combining errors specified per-polarization or per-channel to per-antenna.

Table 5 focuses on the subset of error contributions that can be quantified by delay errors, relevant for both 6 m and 18 m antennas. Tables 6 and 7 present comprehensive comparisons of visibility amplitude error contributions for 6 m and 18 m antennas, respectively. Delay errors have been incorporated into the amplitude error tables by first converting them to phase errors then doubling to yield equivalent amplitude errors (following RD03).

These tables have the potential to be misleading because the error contributions average down over time at different rates. *Interpret with caution.* The tables indicate the approximate relative timescale for averaging spanning fast (seconds to minutes), medium (10's of minutes), slow (hours), and negligible (no significant averaging expected over months). Tropospheric delay measurement errors dominate the comparison tables (by design, to satisfy SYS1501, though over the minimum observing durations explained in the individual derivations).

Component	Contribution (fsec)	Requirement	Averaging Rate
IADCS Tropospheric Delay Measurement Error (Goal)	180	CAL0303	Fast
Antenna Pad Location Residual	60	CAL0311	Slow
Antenna Structure Delay Residual	100	CAL0313	Fast
Electronics Delay Residual	100	CAL0314	Fast

Table 5 Instrumental delay rms noise contributions per 6 m or 18 m antenna (polarization-independent) in 1 sec for a snapshot $M = 1$ observation.

Component	Contribution (%)	Requirement	Averaging Rate
8″ Precision Offset Pointing	0.1	CAL0201	Fast
Primary Beam Model Accuracy	0.2	CAL0203	Slow
Antenna Error Scatter	0.6	CAL0208	Slow
Feed Setting Residual	0.2	CAL0205	Medium
IADCS Tropospheric Delay Measurement Error (Goal)	6	CAL0303	Fast
IADCS Ionospheric Delay Measurement Error (10 sec)	1	CAL0303	Fast
Antenna Pad Location Residual	2	CAL0311	Slow
Antenna Structure Delay Residual	3	CAL0313	Fast
Electronics Delay Residual	3	CAL0314	Fast
Noise Diode Accuracy	0.3	CAL0401	Medium
Antenna Elevation Gain Accuracy	0.2	CAL0402	Slow
Instrumental Bandpass Stability	0.7	CAL0503	Slow
Polarization Leakage Stability	0.2	CAL0604	Negligible
Feed Mechanical Alignment Error	0.06	CAL0609	Negligible
Feed Platform Rotation Error	0.004	CAL0610	Slow

Table 6 Instrumental amplitude error contributions per 6 m antenna (dual-polarization) in 1 sec for a snapshot $M = 1$ observation at spot frequency 27 GHz.

Component	Contribution (%)	Requirement	Averaging Rate
3″ Precision Offset Pointing	0.01	CAL0201	Fast
Primary Meam Model Accuracy	0.2	CAL0203	Slow
Antenna Error Scatter	0.3	CAL0208	Slow
Feed Setting Residual	0.2	CAL0205	Medium
IADCS Tropospheric Delay Measurement Error (Goal)	2	CAL0303	Fast
IADCS Ionospheric Delay Measurement Error (10 sec)	3	CAL0303	Fast
Antenna Pad Location Residual	0.6	CAL0311	Slow
Antenna Structure Delay Residual	1	CAL0313	Fast
Electronics Delay Residual	1	CAL0314	Fast
Noise Diode Accuracy	0.3	CAL0401	Medium
Antenna Elevation Gain Accuracy	0.1	CAL0402	Slow
Instrumental Bandpass Stability	0.3	CAL0503	Slow
Polarization Leakage Stability	0.1	CAL0604	Negligible
Feed Mechanical Alignment Error	0.06	CAL0609	Negligible
Feed Platform Rotation Error	0.004	CAL0610	Slow

Table 7 Instrumental amplitude error contributions per 18 m antenna (dual-polarization) in 1 sec for a snapshot $M = 1$ observation at spot frequency 8 GHz.

6 Verification

The design will be verified to meet the requirements by analysis (A), inspection (I), demonstration (D), or a test (T), each defined below.

Verification by Analysis: The fulfillment of the specified performance shall be demonstrated by appropriate analysis (hand calculations, finite element analysis, thermal modeling, etc.), which will be checked by the ngVLA project office during the design phase.

Verification by Inspection: The compliance of the developed system is determined by a simple inspection (of the design documentation or deliverables) or measurement.

Verification by Demonstration: The compliance of the developed feature is determined by a demonstration.

Verification by Test: The compliance of the developed subsystem with the specified performance shall be demonstrated by an acceptance test (e.g. at factory without integration with interfacing subsystems, or equipment as installed at the site).

Note that a demonstration test verifies design performance, while an acceptance test verifies that the hardware or software destined for installation meets acceptance criteria. All software will be subject to acceptance testing.

Multiple verification methods are allowed over the course of the design phase. The final verification method is identified below.

Req #	Parameter/Requirement	A	I	D	T
CAL0201	Antenna Pointing				*
CAL0202	Spectral Line Noise Leakage (Arising From Pointing)				*
CAL0203	Primary Beam Model Accuracy				*
CAL0204	Antenna Aperture Plane Error				*
CAL0208	Antenna Error Scatter Pattern				*
CAL0205	Feed Setting Calibration Residual				*
CAL0206	Band Switching				*
CAL0207	Antenna Motion				*
CAL0303	Atmospheric Delay Calibration Residual				*
CAL0304	Tropospheric Delay Measurement Capability		*		
CAL0305	Amplitude and Phase Coherence Over Multiple Observations				*
CAL0306	Ionospheric Delay Measurement				*
CAL0307	Ionospheric Disturbance Monitoring				*
CAL0308	Proposal Content: Estimated Dynamic Range		*		
CAL0309	Scheduler Start/Stop/Restart				*
CAL0310	Interplanetary Medium Monitoring				*
CAL0301	Geometric Delay Calibration Residual				*
CAL0315	Delay Model Accountability		*		
CAL0302	Coordinate Equinox		*		
CAL0311	Antenna Pad Location Calibration Residual				*
CAL0312	Timing Accuracy Across Baselines				*
CAL0313	Antenna Structure Delay Calibration Residual				*

Req #	Parameter/Requirement	A	I	D	T
CAL0314	Electronics Delay Calibration Residual Per Polarization				*
CAL0401	Noise Diode Amplitude Stability				*
CAL0402	Antenna Elevation Gain Amplitude Dependency				*
CAL0403	Default Amplitude Calibration				*
CAL0404	Calibrator Database: Flux Density Standards		*		
CAL0405	Internal Absolute Amplitude Scale				*
CAL0406	Switched power RFI mitigation				*
CAL0501	Default Bandpass Calibration				*
CAL0502	Instrumental Bandpass Accuracy		*		
CAL0503	Instrumental Bandpass Stability			*	
CAL0504	Calibration Database: Bandpass		*		
CAL0505	Proposal Content: Estimated Dynamic Range Per Channel		*		
CAL0601	Feed Basis		*		
CAL0602	Default Polarization Calibration				*
CAL0603	Polarization Leakage Accuracy		*		
CAL0604	Polarization Leakage Stability			*	
CAL0605	Calibration Database: Polarization Leakages		*		
CAL0606	Calibrator Database: Polarization Calibrators		*		
CAL0607	Relative Gain Amplitude Stability				*
CAL0608	Crosshand Bandpass Phase Stability				*
CAL0609	Feed Mechanical Alignment				*
CAL0610	Rotation of Feed Platform				*
CAL0611	Pipeline Ingestion of GPS VTEC				*
CAL0612	Antenna Re-Calibration Following Maintenance	*			
CAL0701	Calibrator Search and Characterization				*
CAL0702	Modeling of Calibrator Structure				*
CAL0703	Array Configuration Snapshot Performance	*			
CAL0704	Calibrator Database: Source Ingest				*

7 APPENDIX

7.1 Abbreviations & Acronyms

Acronym	Description
ALMA	Atacama Large Millimeter/submillimeter Array
CASA	The Common Astronomy Software Applications package
DIXSG	Disturbance ionosphere index spatial gradient
EVLA	Expanded Very Large Array
FWHM	Full-width at half-maximum
GDGPS	Global Differential GPS System
GPS	Global Positioning System
HPBW	Half-power beam-width
IADCS	Independent atmospheric delay calibration subsystem
IAU	International Astronomical Union
ICRF	International Celestial Reference Frame
IF	Intermediate frequency
IGRF	International Geomagnetic Reference Field
IGS	International Global Navigation Satellite System Service
IRD	Integrated Receiver and Downconverter
JPL	Jet Propulsion Laboratory
JVLA	Jansky Very Large Array
LBA	Long Baseline Array
MA	Main Array
MAPGPS	MIT Automated Processing of GPS
MIT	Massachusetts Institute of Technology
RF	Radio frequency
RFI	Radio frequency interference
rms	Root mean square
ROTI	Rate of TEC index
SBA	Short Baseline Array
SNR	Signal to noise ratio
STEC	Slant total electron content
TEC	Total electron content
TECU	Total electron content unit

Acronym	Description
uv	Spatial frequency plane coordinates
VTEC	Vertical total electron content
VLBA	Very Long Baseline Array
VLBI	Very long baseline interferometry
WVR	Water vapor radiometer/radiometry